Unravelling the timing and distribution of Paleoproterozoic dyke swarms in the eastern Kaapvaal Craton, South Africa

Camilo Esteban Gaitan Valencia

Dissertations in Geology at Lund University,
Master's thesis, no 578
(45 hp/ECTS credits)

Department of Geology
Lund University
2019

Unravelling the timing and distribution of Paleoproterozoic dyke swarms in the eastern Kaapvaal Craton, South Africa

Master's thesis

Camilo Esteban Gaitan Valencia

Department of Geology
Lund University
2019

Contents

1 Introduction **7**
2 Regional Geology **8**
2.1 Pretoria Group 8
3 Sample localities **9**
3.1 KwaZulu Natal Province 9
3.1.1 ENED-03 and ENED-03R 9
3.1.2 ENED-03S and ENED-03SN 11
3.2 Mpumalanga Province 12
3.2.1 BCD8-05 12
3.2.2 BCD18-05B 12
4 Methodology and analytical Protocol **13**
4.1 Geochronology 13
4.2 Geochemistry 13
5 Results **13**
5.1 Geochronology 13
5.1.1 BCD18-05B 13
5.1.2 ENED-03 15
5.1.3 ENED-03S 15
5.1.4 BCD8-02 15
5.2 Geochemistry 15
6 Discussion **16**
6.1 U-Pb data interpretation 16
6.2 Timing and geochemistry of the Mashining event 17
6.3 Timing and geochemistry of the Black Hills event 17
6.4 New definition of dyke swarms in eastern Kaapvaal Craton 19
6.5 Potential global correlations 20
7 Conclusions **21**
8 Acknowledgements **21**
9 References **21**

Cover Picture: Mafic black dyke intruding a white host granitic rock. Photo taken by Ashley Gumsley.

Unravelling the timing and distribution of Paleoproterozoic dyke swarms in the eastern Kaapvaal Craton, South Africa

CAMILO ESTEBAN GAITAN VALENCIA

Gaitan Valencia, Camilo E., 2019: Unravelling the timing and distribution of Paleoproterozoic dyke swarms in the eastern Kaapvaal Craton, South Africa. *Dissertations in Geology at Lund University*, No. 578, 23 pp. 45 hp (45 ECTS credits).

Abstract: In this study, I present emplacement ages, petrography and the geochemical composition of doleritic dykes and one sill from the eastern and south-eastern area of the Kaapvaal Craton. These results refine the previous 2253 ± 45 and 2202 ± 74 Ma ages of the Mashining event to ca. 2168 Ma, and shows that this swarm is intermixed with the younger 1875-1835 Ma Black Hills dyke swarm. Geochemical data of the Mashining swarm suggest these dykes may acted as feeders of ca. 2.2 Ma Hekpoort magmatism within the Pretoria Group. A Southern extension of Mashining magmatism in the Kaapvaal Craton is represented by the ENED-03 dyke, herein dated to 2168 ± 7 Ma. However, despite this age match, there are considerable geochemical differences. The trend of the Black Hills dyke parallels the older ca. 2168 Ma Mashining dykes within the Transvaal sub-basin. Further north, in the area of the Archean basement, it extents close to the ca. 1.85 Ga Soutpansberg Group basin, suggesting a possible connection and a common magmatic event. The northerly trend of Black Hills dykes just northeast of the Transvaal sub-basin seems to be locally deflected by older NE-trending fracture zones and dykes that belong to a major ca. 2.70-2.66 Ga NE-trending swarm. Echelon and dyke patterns, thus suggest that the trend of Black Hills dykes in that area was controlled by former regional paleo-stresses and fracture zones. The definition of the ca. 2168 Ma age for the Mashining magmatic event on the Kaapvaal Craton indicates possible connection to coeval magmatic events in the Wyoming, Dharwar and Superior Cratons.

Keywords: Kaapvaal, Mashining, Black Hills, dyke events, U-Pb geochronology, baddeleyite, geochemistry.

Supervisor(s): Ulf Söderlund (Lund University) and Ashley Gumsley (Lund University)

Subject: Bedrock Geology

Camilo Esteban Gaitan Valencia, Department of Geology, Lund University, Sölvegatan 12, SE-223 62 Lund, Sweden. E-mail: ca3263ga-s@student.lu.se

Paleoproterzoiska diabasgångsvärmar i östra Kaapvaal kratonen, Sydafrika – deras kristallisationsåldrar och geografiska utbredning

CAMILO ESTEBAN GAITAN VALENCIA

Gaitan Valencia, Camilo E., 2019: Avslöja tidpunkten och distributionen av Paleoproterozoic dyke svärmar i östra Kaapvaal Craton, Sydafrika.*Examensarbeten i geologi vid Lunds universitet*, Nr. 578, 23 sid. 45 hp.

Sammanfattning: I denna uppsats presenterar jag kristallisationsåldrar, petrografi och geokemisk sammansättning för diabasgångar och en lagergång i östra och sydöstra Kaapvaal kratonen, Sydafrika. Dessa nya resultat ger mer exakta och pålitliga resultat än tidigare dateringar för diabaser tillhörande den s.k. Mashining gångsvärmen, vilka daterats till 2253 ± 45 and 2202 ± 74 Ma (Ma = miljoner år). De nya resultaten indikerar en ålder på ca. 2168 Ma, samt att denna generation av Mashining diabaser förekommer i samma område som yngre diabasgångar tillhörande den s.k. Black Hills svärmen, vilken tidigare åldersbestämts till 1875-1835 Ma. Geokemisk data indikerar att Mashining diabaserna kan ha utgjort matargångar till de berömde Hekpoort basalterna som återfinns i ”Pretoria Group” i Transvaal bassängen. En diabasgång belägen betydligt längre söderut ger en liknande ålder runt 2168 Ma och visar att denna händelsen sannolikt var av regional betydelse. Den nordliga fortsättningen av 1875-1835 Ma Black Hills gångar sammanfaller med vulkaniska bergarter i den s.k. Southpansberg bassängen i norr, vilka daterats till ca. 1.85 Ga (Ga = miljarder år), och indikerar en möjlig koppling mellan intrusiva och extrusiva bergarter tillhörande en och samma magmatiska händelse. Det finns också möjliga kopplingar till likåldriga magmatiska provinser/diabasgångsvärmar i Wyoming, Dharwar och Superior kratonerna, vilket kan tolkas som att dessa kratoner var belägna i närheten av Kaavaal kratonen för ca 2 miljarder år sedan.

Nyckelord: Kaapvaal, Mashining, Black Hills, intrusioner händelser, U-Pb geokronologi, baddeleyit, geokemi

Handledare: Ulf Söderlund (Lunds Universitet) och Ashley Gumsley (Lunds Universitet)

Ämnesinriktning: Berggrundsgeologi

Camilo Esteban Gaitan Valencia, Geologiska institutionen, Lunds Universitet, Sölvegatan 12, 223 62 Lund, Sverige. E-post: ca3263ga-s@student.lu.se

1 Introduction

The study of dyke swarms along the margin and within cratons has become one of the most useful techniques for reconstructions of supercontinents in the Precambrian (e.g. Bleeker 2004; Ernst et al. 2013; Ernst 2014; Söderlund et al. 2016). Dyke swarms are made up of a series of dykes with a specific trend and pattern (e.g. linear or radiating). The dykes typically belong to a single magmatic event of intrusion, but multiple generations of dykes within single swarms are not uncommon (e.g. Olsson et al. 2011;Cederberg et al. 2016). Many of these swarms are associated with Large Igneous Provinces (LIPs) and, if radiating, often are inferred to be linked to a mantle plume causing extensive magmatism within a relatively short time span (1-5 Myr;e.g. Emst & Buchan 2001; Bryan & Ernst 2008; Ernst 2014). It is widely accepted that one or several mantle plumes could lead to continental break up and initiate rifting. Ancient events of mafic magmatism can be arranged in so called "magmatic barcodes" for each craton (e.g. Bleeker & Ernst 2006). One or several age matches between crustal blocks suggest a "nearest neighbor" relationship within the time interval in which matches are identified.

The Kaapvaal Craton in southern Africa represents one of the oldest pieces of crust on Earth, and is the host of a large number of dyke swarms each representing events of extensional stress and/or magmatism (Fig. 1). In the eastern part of the craton, within the Archean crust, three regional swarms dominate, all comprising ca. 2.70-2.66 Ga dykes that are arranged in a radial pattern (Olsson et al. 2011): the NE-trending Rykoppies dyke swarm and the SE-trending Badplaas-Barberton dyke swarm. The latter is intermixed with older, ca. 2.97-2.96 Ga dykes, whereas the NE-trending swarm is intermixed with younger 1.875-1.835 Ga dykes, referred to as the Black Hills dyke swarm (Olsson et al. 2016). As dykes of the NE-trending swarm intersect the Transvaal Supergroup, the dykes appear to become deflected into a more NNE-trend toward the south. However, there are some uncertainties whether this deflection is apparent or if more than one generation of various trends is present in this part of the craton. The NNE-trending dykes within the Transvaal Supergroup (near Mashining) were recently defined by Wabo et al. (2019) as the Mashining dyke swarm, and $^{40}Ar/^{39}Ar$ geochronology indicated an age of ca. 2.2 Ga. Further south the White Mfolozi dyke swarm has been defined as a NE-trending swarm dated at ca. 2.7 Ga (Gumsley et al. 2016), but other generations of dykes also exist in this part of the craton. For instance, Larsson (2015) defined three ENE-trending generations of dykes (sample names from (Larsson 2015)): one dated at ca. 2.73 Ga (ENED-08), a second at ca. 2.58 Ga (ENED-09), and the youngest at ca. 2.168 Ga (ENED-03), the latter similar in age to the Mashining swarm defined further north (Wabo et al. 2019). These ca. 2.2 Ga dykes may have acted as feeder dykes to Hekpoort, or Machadodorp, lavas within the Transvaal Supergroup.

The aim of this study is to refine the definition and improve the understanding of different dyke swarms in the eastern Kaapvaal Craton. More specifically, this study seeks the answers to: (1), what is the spatial and temporal relationship between the 1.875-1.835 Ga Black Hills dyke swarm and the Mashining dyke swarm, provisionally dated at ca. 2.2 Ga, (2), could any of these dyke swarms represent feeder dykes of the Hekpoort or Machadodorp lavas, and (3), what is the extent of ca. 2.2 Ga magmatism in the eastern Kaapvaal Craton. In order to answer these questions, U-Pb geochronology was done on baddeleyite using isotope dilution-thermal ionization mass spectrometry

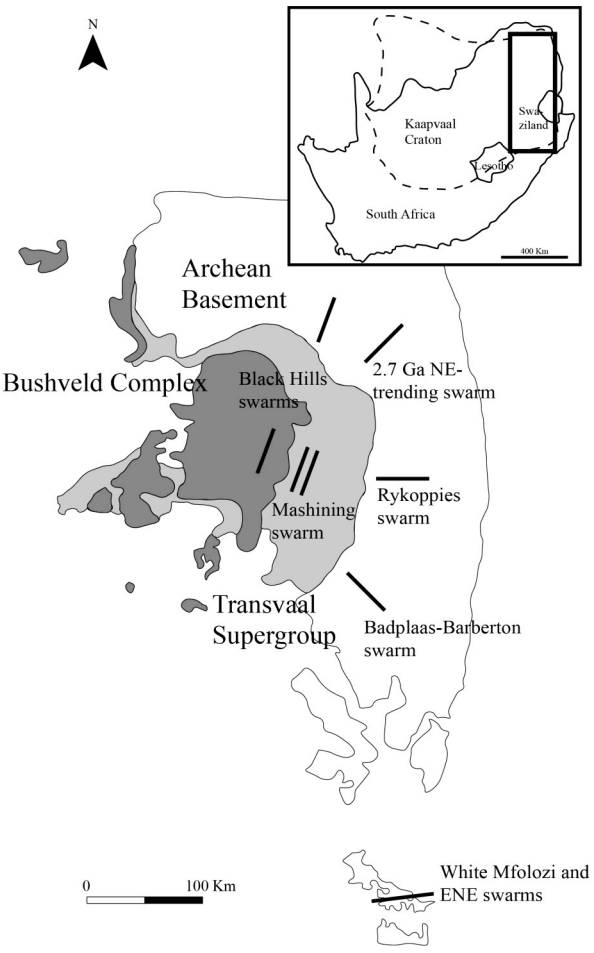

Fig. 1. Geographical distribution of the main dyke swarms in the eastern area of the Kaapvaal Craton. Each bar represents the main trend of dykes for certain generation. Note that there are three bars representing the Black Hills swarm, one in the Archean Basement, one in the Transvaal Supergroup and one in the Bushveld Complex. Modified from Larsson (2015), Gumsley (2015) and Eriksson (2006).

(ID-TIMS), combined with petrography and geochemistry on samples of different trends and generations.

2 Regional Geology

The late Neoarchean to early Paleoproterozoic Transvaal Supergroup (Fig. 2) occurs in southern Africa in three sub-basins unconformably overlying the Ventersdorp Supergroup on the Kaapvaal Craton. These are the Kanye, Griqualand West and Transvaal sub-basins. The Transvaal sub-basin is a relatively thick (~ 15 km) succession that outcrops around the ca. 2058 Ma Bushveld Complex (Buick et al. 2001; Olsson et al. 2010; Cawthorn 2015) in the north-eastern part of the Kaapvaal Craton. The basement in this region includes the Ventersdorp Supergroup and the sporadic so-called protobasinal rocks. Overlying these units unconformably is the first succession of the sub-basin, the Black Reef Formation, which comprises a mixture of conglomerates, sandstones and volcanic rocks. Overlying the Black Reef Formation is the Chuniespoort Group (Eriksson et al. 2006). This comprises a series of carbonate platform deposits of the Malmani Subgroup, the banded iron formations from the Penge Formation and a sporadic carbonate succession on top, the Tongwane Formation (Schröder & Warke 2016). Unconformably overlying the Chuniespoort Group is the Duitschland Formation, some studies (Coetzee 2001; Luo et al. 2016; Schröder et al. 2016; Warke & Schröder 2018) have correlated the Duitschland Formation with the Rooihoogte Formation from the overlying Pretoria Group. This correlation is not fully accepted, and some workers have instead interpreted the Duitschland Formation as part of the Chuniespoort Group (Catuneanu & Eriksson 2002; Eriksson et al. 2006). A third alternative suggests that the Duitschland Formation represents an unconformably-bounded unit between the Chuniespoort Group and the Pretoria Group (Lenhardt et al. 2012; Gumsley et al. 2017). This is the alternative favored in this thesis.

2.1 Pretoria Group

The mafic intrusions investigated in this study, correspond temporally to the Pretoria Group, which has a stratigraphy as is seen in Figure 3. The Pretoria Group unconformably overlies the Duitschland Formation and is the third succession in the Transvaal sub-basin. The lower Pretoria Group is divided into four formations. The lowermost unit, the Rooihoogte Formation, consists of shales with some conglomerates and breccias towards the top (Coetzee 2001). Above this succession is the Timeball Hill Formation, which contains two upwards coarsening units of shale separated by a sandstone unit and a diamictite unit on top (Coetzee 2001; Coetzee et al. 2006). The base of the unit has been dated at 2316 ± 7 Ma (Re-Os on pyrite; Hannah et al. 2004) and 2309 ± 7 Ma (U-Pb on zircon; Rasmussen et al. 2013), whereas the upper part has been dated at 2256 ± 6 Ma and 2266 ± 4 Ma (U-Pb on zircon; Rasmussen et al. 2013). Unconfor-

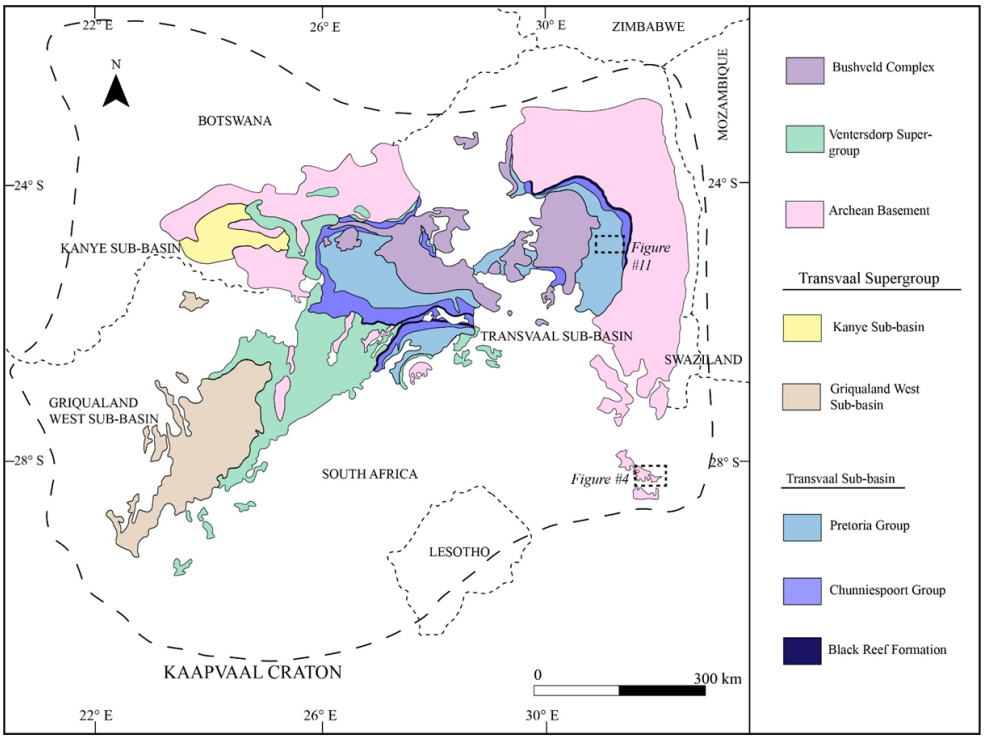

Fig. 2. Geological map of the main units in the studied zone over the Kaapvaal Craton. The two localities carried out in this study are marked by the black boxes referring to Figure 4 and 11. Modified from Larsson (2015), Gumsley (2015) and Eriksson (2006).

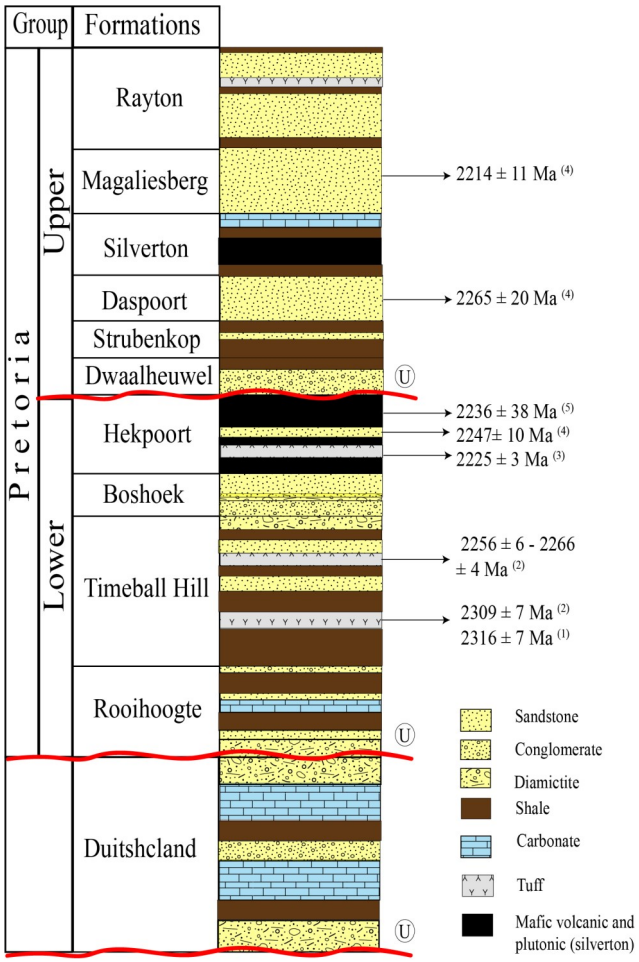

Fig. 3. Schematic log from the Pretoria Group. Published ages are from: 1) Hannah et al. (2004); 2) Rasmussen et al. (2013); 3) Dorland (2004); 4) Schröder et al. (2016); 5) Cornell et al. (1996). U represents an unconformity.

mably overlying this succession is the Boshoek Formation, a clastic unit consisting of conglomerates, diamictites and sandstones (Coetzee 2001; Coetzee et al. 2006; Schröder et al. 2016; Gumsley et al. 2017). Further upwards in the stratigraphy is the Hekpoort Formation, a volcanic unit dominated by basaltic andesites and volcanoclastic sedimentary rocks (Oberholzer & Eriksson 2000; Coetzee 2001; Lenhardt et al. 2012; Schröder et al. 2016). The age of this unit is not well-constrained, but some attempts to date the Hekpoort Formation have been done: 2236 ± 38 Ma (Pb-Pb on whole rock; Cornell et al. 1996); 2225 ± 3 Ma (Pb-Pb on detrital zircon; Dorland 2004), the latter yielding a maximum depositional age, and 2247 ± 10 Ma (U-Pb on zircon; Schröder et al. 2016). Similarly, this age represents a maximum depositional age for volcanoclastic quartzites in the Hekpoort Formation.

Unconformably overlying the Hekpoort Formation is the upper Pretoria Group. This begins with the Dwaalheuwel Formation, comprised of shales and conglomerates, followed by the Strubenkop Formation shales and some subordinate sandstone layers, and then the Daspoort Formation, which consists of sandstones with minor shale layers (Coetzee 2001; Eriksson et al. 2006). This latter unit has been dated at 2265 ± 20 Ma (U-Pb on detrital zircon; Schröder et al. 2016), representing a maximum depositional age of the Daspoort Formation. Above this formation is the Silverton Formation which is, primarily composed of shale and carbonate rocks. However, it also includes a volcanic unit called the Machadodorp Member, composed of pyroclastic rocks on the base, followed by lava flows and pillow lavas toward the top (Crow & Condie 1990; Reczko et al. 1995; Lenhardt et al. 2012). Overlying the Silverton Formation is the Magaliesberg Formation, which is composed of sandstones layers with some interbedded shale lenses (Coetzee 2001; Eriksson et al. 2006; Schröder et al. 2016). This formation has yielded a maximum age of 2214 ± 11 Ma (U-Pb on detrital zircon; Schröder et al. 2016). Finally, overlying these formations are a series of other formations (the Vermont, Lakenvalei, Nederhorst, Steenkampsberg and Houtenbek), which comprise mainly sandstones with some shale layers and rare tuffs. These formations are grouped into a single formation which Eriksson et al. (2006) refers to as the Rayton Formation.

Sedimentation on the Transvaal sub-basin and the Transvaal Supergroup was terminated by the intrusion of the ca. 2.05 Ga Bushveld Complex and related volcanic activity of the Rooiberg Group (Walraven 1997; Olsson et al. 2010; Olsson et al. 2011; Zeh et al. 2015).

3 Sample Localities

3.1 KwaZulu Natal Province

Sampling in this province was carried out along the White Mfolozi River (Fig. 4). One dolerite sill (samples ENED-03S and ENED-03SN) and one gabbroic dyke (samples ENED-03 and ENED-03R) were collected. In this province granitic Archean rocks predominate as host rock to a series of ~20 m wide ENE-trending mafic dykes. Dolerite and sills classified as part of the Karoo volcanism cut both the granitic rock and the mafic dykes (Frick 1988).

3.1.1 ENED-03 and ENED-03R

The two samples ENED-03 and ENED-03R were collected from a ~20 m wide black doleritic dyke trending 85°. It intrudes the granitic host rock and is cut by a blocky doleritic sill (Fig. 5). This dyke was previously investigated by Lubnina et al. (2010) and Larsson (2015), and they referred to this dyke as NL-14 and ENED-03 respectively. ENED-03R was taken

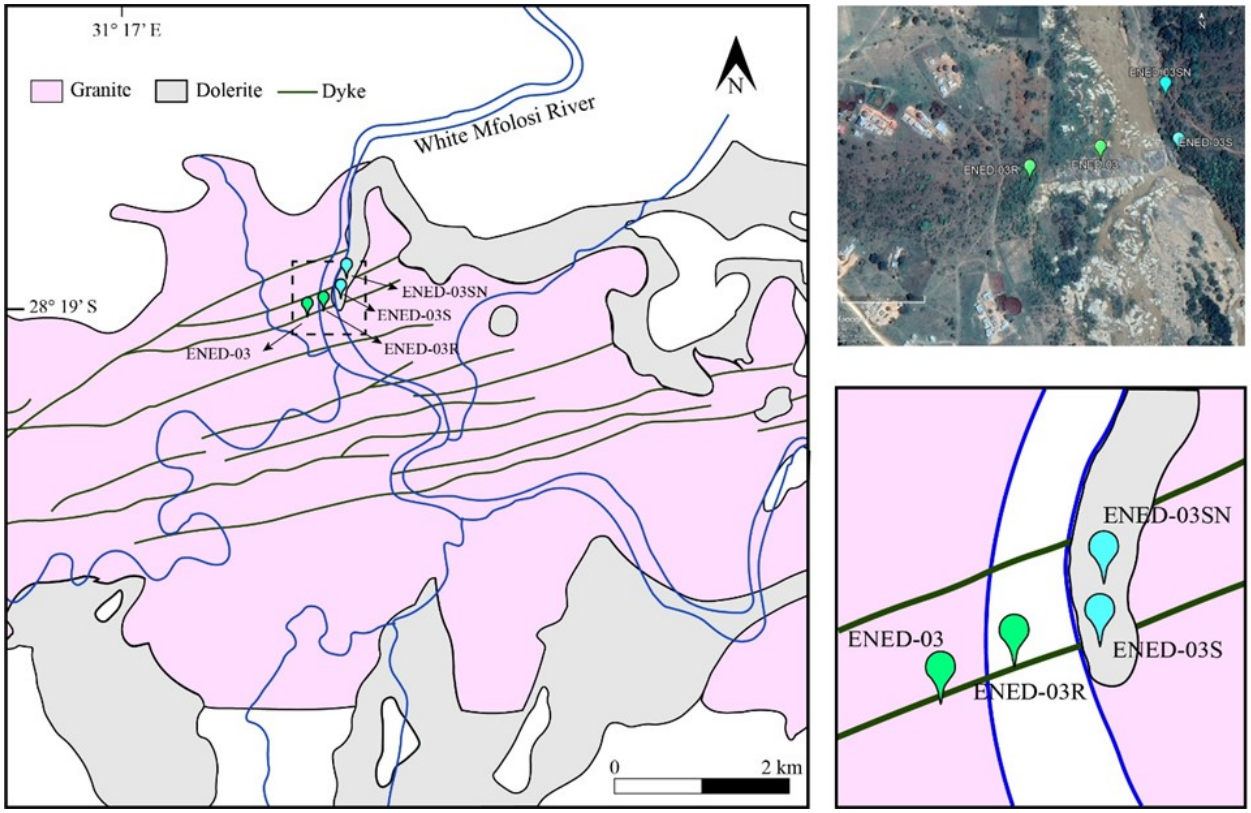

Fig. 4. Simplified geological map and Google Earth image of the studied area in KwaZulu Natal province. It illustrates the main units and the location of the samples. Image on the bottom-right zoom in is the distribution and detailed location of the samples collected. Modified after 1:250 000 geological series map 2830 – Dundee from the Council for Geoscience.

Fig. 5. Dyke of samples ENED-03 and ENED-03R seen from the east side of the river. It is a mafic dyke ~20 m wide trending 85°, its contact with the host rock (granitic white rock) is clear at both sides of the image. In the bottom part of the image it can be observed the blocky brownish sill. Photo taken by Ashley Gumsley.

~20 m east of the ENED-03 sampling site. The dyke displays a clear phaneritic crystallinity and an intergranular texture. Its major mineral phases are subhedral to euhedral clinopyroxenes and plagioclase laths often altered (Figs. 6 and 7). Alteration minerals include sericite and, chlorite, with some amphiboles.

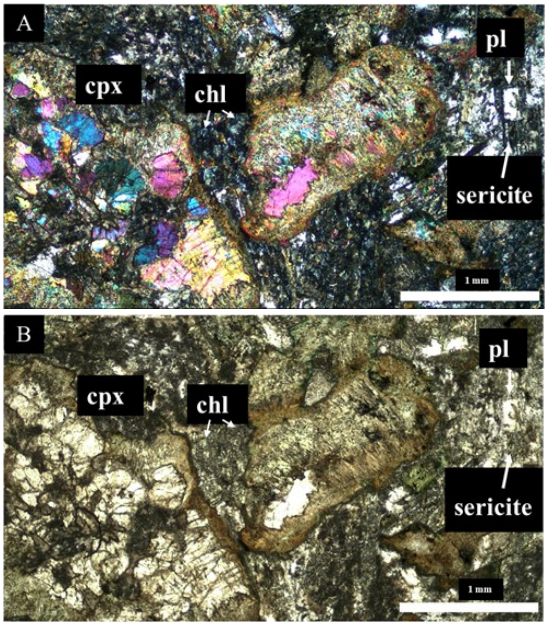

Fig. 6. Microscopy images of thin section of sample ENED-03. **A)** CPL image showing the general texture of the section with strongly altered clinopyroxene and sericitized plagioclase. **B)** In PPL image can be appreciated easier the alteration in the dark brown zones at the edges of the crystals.

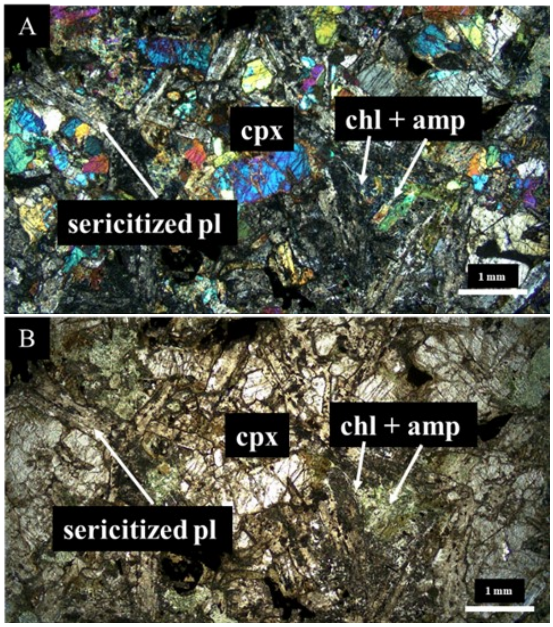

Fig. 7. Microscopy photographs of sample ENED-03R. **A)** CPL image showing the general texture with the major mineral components, clinopyroxene and plagioclase, the plagioclase is highly broken down into sericite and some of the clinopyroxenes are broken down into chlorite and amphiboles. **B)** In PPL image can be appreciated easier the alteration, it can also be distinguished the PPL colors from the chlorite and the amphiboles

3.1.2 ENED-03S and ENED-03SN

These samples were collected from a sill subhorizontally overlying the described mafic dyke (Fig. 8). The sill has a brownish blocky appearance and it shows a phaneritic granularity with an intergranular texture. Sample ENED-03S does not show signs of alteration (Fig. 9) while ENED-03SN displays moderate alteration (Fig. 10). The major mineral phases are

Fig. 8. This image shows the sub-horizontal contact between the brownish blocky doleritic sill that is overlying the gabbroic dyke. This is the east side of the river where samples ENED-03S (from the sill) and ENED-03 (from the dyke) were taken. Photo taken by Anna Salacinska.

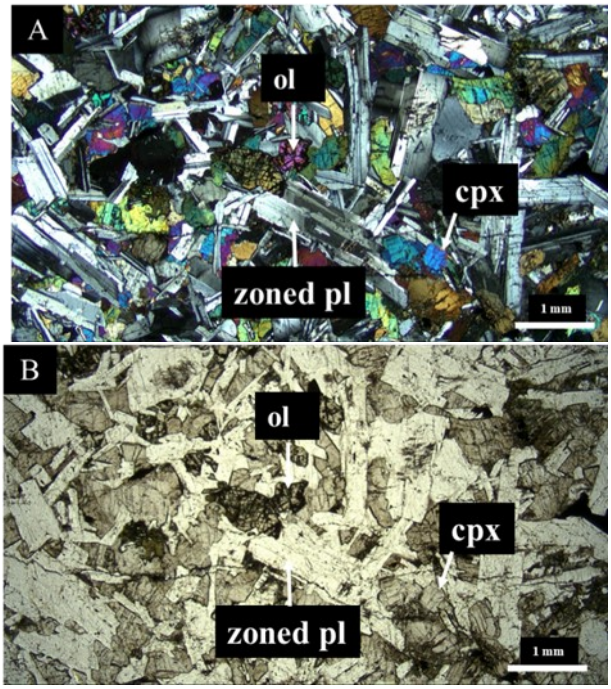

Fig. 9. Microscopy photographs of sample ENED-03S. CPL (A) and PPL (B) images shows the intergranular texture of the sill. The major mineral phases are clinopyroxenes and plagioclase laths, some scarce olivine and alteration minerals are in the sample as well.

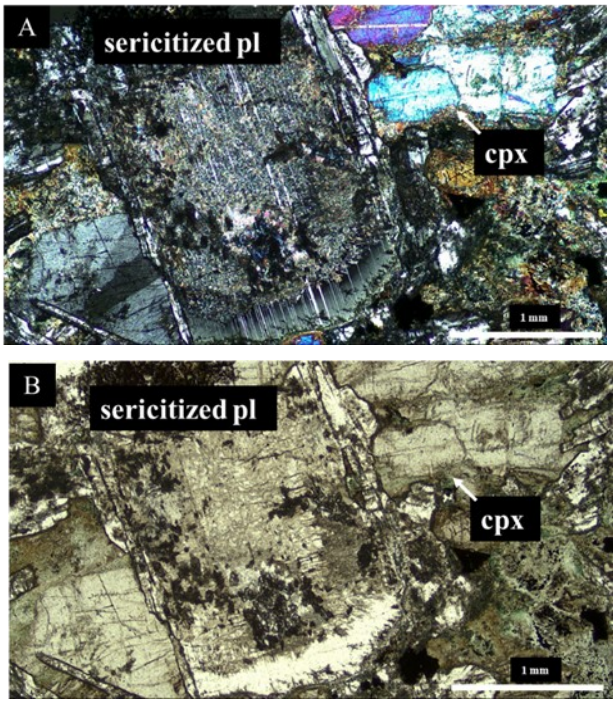

Fig. 10. Microscopy photographs of sample ENED-03SN. CPL(A) and PPL(B) image showing the sericitization process in a plagioclase crystal. Unlike the previous sill sample this one is more altered.

euhedral clinopyroxenes, zoned plagioclase laths and some scarce and small olivines. Minor sericite and chlorite can also be seen in the samples.

3.2 Mpumalanga Province

Sampling in this province was done in dykes cropping out in valleys in the Mashining area near to the Klein Spekboom river (Fig. 11). Sample BCD8-05 was collected by Johan Olsson in 2008 whereas sample BCD18-05B was collected by Ashley Gumsley in 2018. The geology in this province is dominated by

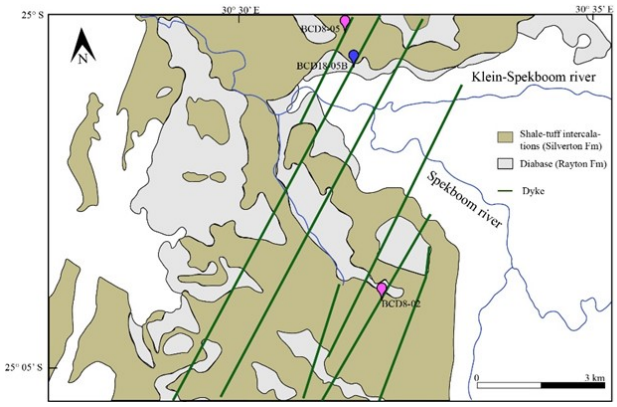

Fig. 11. Simplified geological map of the studied area in Mpumalanga province. It illustrates the main units and the location of the samples. Modified after 1:250 000 geological series map 2530 – Barberton from the Council for Geoscience.

diabases within the Rayton Formation, and shales and tuff layers from the Silverton Formation. These are cross-cut by ~40 m wide NNE-trending mafic dyke (Smit 1986).

3.2.1 BCD8-05

This dyke displays a phaneritic granularity with an intergranular texture (Fig. 12). The major mineral phases are ribbon-elongated clinopyroxenes with highly altered plagioclase. Other minor components are opaque minerals, sericite, chlorite, iron oxides and baddeleyite within quartz crystals (Fig. 12).

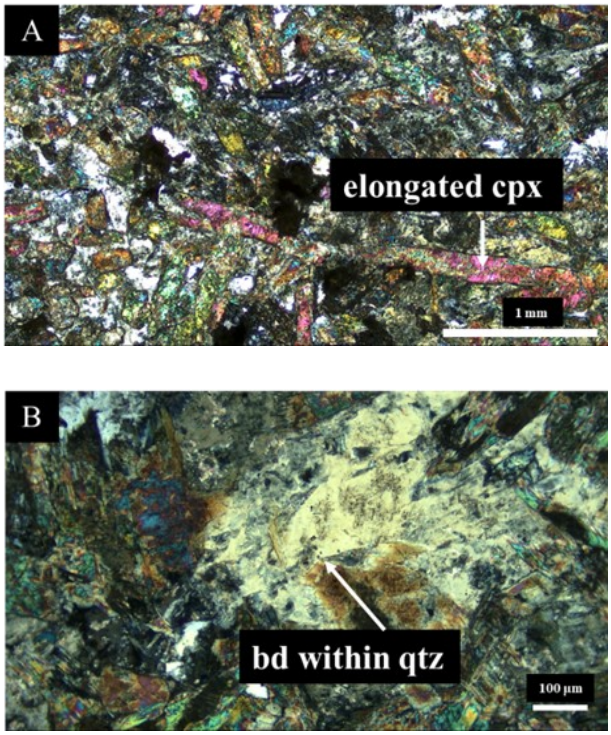

Fig. 12. Microscopy photographs of dyke BCD8-05. **A)** CPL image showing a highly altered intergranular texture and ribbon-elongated clinopyroxenes. **B)** CPL image showing baddeleyite crystals found within a quartz crystal.

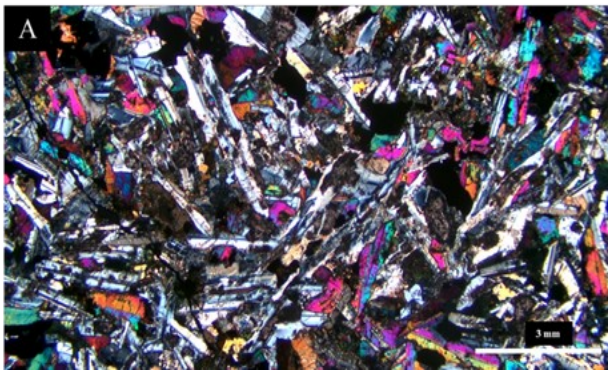

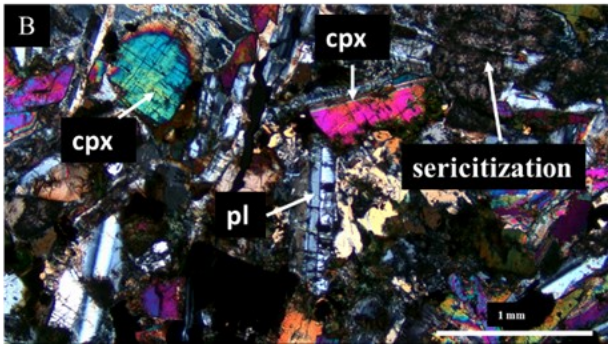

Fig. 13. Microscopy photographs of dyke BCD18-05B. **A)** CPL image showing the intergranular texture, note that unlike the previous sample this is less altered and clinopyroxenes are not as elongated. **B)** CPL image showing the major mineral components of the dyke, clinopyroxenes and plagioclase laths. Minor sericitization on plagioclases can be appreciated as well

3.2.2 BCD18-05B

This dyke shows a phaneritic granularity with an intergranular texture (Fig. 13). The major mineral phases are subhedral elongated clinopyroxenes and euhedral plagioclase laths. Other minor minerals including opaque minerals, sericite, chlorite and some amphiboles can be found as well.

4 Methodology and analytical protocol

4.1 Geochronology

Samples were sawed to remove the most altered zones and to split them into smaller pieces before crushing. The smaller pieces were crushed using a sledgehammer into pieces less than 1 cm^3. Powder was produced using an ordinary chrome-steel swing mill. Before transferring the powder onto the Wifley water-shaking table, water plus a few drops of soap were added, the latter in order to reduce adhesive forces between grains. Approximately one spoon of the suspended sample (ca 15 grams) was loaded onto the Wifley table. After 2-3 minutes most of the coarser material had been washed off and the finest material remaining was collected in a plastic beaker following the methodology described in Söderlund& Johansson (2002). The collected material was dominated by the smallest and densest minerals, i.e. Fe-oxides and sulphides, apatite and, baddeleyite. That heavy mineral fraction was carefully transferred into a glass Petri dish. A hand magnet wrapped in thin plastic cover was used to remove the magnetic minerals. Baddeleyite was handpicked under microscope, and the best quality grains were transferred into a new plastic Petri dish.

In the clean lab, the baddeleyite grains were divided into fractions comprising 1 to 3 grains in each, before being transferred into pre-washed Teflon capsules. The grains were washed in several steps by adding and removing of 7N HNO_3 and H_2O between each step. One cleaning step was performed in 3.5 N HNO_3 on hot plate at ca. 80 °C for ~1 hour. Finally, one drop of $^{233\text{-}236}U$ ^{205}Pb spike solution was added together with 10 drops of 14 M HF and 1 drop of 3.5 N HNO_3. Last, the Teflon capsules were placed into steel jackets and then put in the oven at ~ 190 °C for 2-3 days to ensure complete isotopic homogenization of the U and Pb in the sample and spike.

At the Swedish Museum of Natural History, the capsules were opened and put on hot plate to evaporate the HF-HNO_3 solution. Once dried down, 10 drops of 6.1 M HCl and one drop of 0.125 M H_3PO_4 were added to each sample, and thereafter left on the hot plate. The tiny "phosphatic" drops were mixed with 2 µl of silica gel and put onto outgassed Rhenium filaments. On the filaments, the gel is progressively heated at a current starting at 1 A, finishing when the H_3PO_4 burns off at ~2.4 A, when the sample turns into a white crust. Filaments are assembled in the ion source of the TIMS Finnigan Triton mass spectrometer for analysis. The isotopic ^{204}Pb, ^{254}Pb, ^{206}Pb, ^{207}Pb and ^{208}Pb were measured at temperatures between 1180 and 1250 °C. Samples yielding high intensities were measured using Faraday Cups whereas for low-intensity samples signals were measured in peak-jumping mode using a SEM (Secondary Electron Multiplier). The ^{233}U, ^{236}U and ^{238}U were measured at temperatures between 1280 -1350 °C in peak-jumping mode. Finally, data corrections and reporting was done using the Microsoft Excel based program Isoplot (Ludwig 2003).

4.2 Geochemistry

The samples were sawed and crushed to smaller fractions using a sledge hammer and a mallet. A fine powder was produced using a tungsten-carbide swing mill. Between samples, the tungsten-carbide mill was carefully washed in water with soap to avoid sample contamination. From each sample approximately 10 grams of powder were sent to the Bureau Veritas Laboratories in Canada. XRF analyses (X-ray fluorescence) were carried out for major and minor oxides and ICP-MS (Inductively coupled plasma mass spectrometry) analyses for trace elements. The loss on ignition (LOI) was also measured and reported. The samples in which the analyses were performed were: ENED-03, ENED-03R, ENED-03S, BCD8-02 and BCD18-05B.

Table 1 . U-Pb TIMS data

Analysis no. (number of grains)	U/ Th	Pbc/ Pbtot[1)]	$^{206}Pb/^{204}Pb$ raw[2)]	$^{207}Pb/^{235}U$	± 2s % err	$^{206}Pb/^{238}U$ [corr][3)]	± 2s % err	$^{207}Pb/^{235}U$	$^{206}Pb/^{238}U$	$^{207}Pb/^{206}Pb$ [age, Ma]	± 2s	Concord-ance
BCD18-05B												
Bd-a (3 grains)	18.2	0.067	941.2	4.9030	0.84	0.31542	0.80	1802.8	1767.3	1844.0	5.4	0.958
Bd-b (1 grain)	13.5	0.041	1590.5	5.1356	0.61	0.32960	0.60	1842.0	1836.4	1848.3	3.2	0.994
Bd-c (3 grains)	2.9	0.486	77.7	5.1443	0.86	0.32912	0.64	1843.5	1834.1	1854.0	10.4	0.989
ENED-03												
Bd-a (8 grains)	6.9	0.096	601.3	7.2066	0.82	0.38675	0.79	2137.3	2107.7	2165.9	4.9	0.973
Bd-mff (5 grains)	7.7	0.211	250.2	6.8964	1.32	0.36960	1.14	2098.2	2027.5	2168.3	12.0	0.935
Bd-mff2 (3 grains)	n.m.	0.272	243.6	6.5558	3.19	0.35350	3.19	2053.4	1951.3	2157.6	14.9	0.904
Bd-c (3 grains)	6.7	0.144	451.0	6.4606	2.18	0.34775	2.16	2040.6	1923.8	2160.7	10.6	0.890
BCD8-02												
Bd-a (1 grain)	0.6	0.664	43.3	8.0649	2.74	0.43262	2.34	2238.3	2317.5	2166.6	27.5	1.070

[1)] Pbc = common Pb; Pbtot = totalPb (radiogenic + blank + initial).

[2)] measured ratio, corrected for fractionation and spike.

[3)] isotopic ratios corrected for fractionation (0.1% per amu for Pb), spike contribution, blank (0.6 pg Pb and 0.06 pg U), and initial common Pb. Initial common Pb corrected with isotopic compositions from the model of Stacey and Kramers (1975) at the age of the sample.

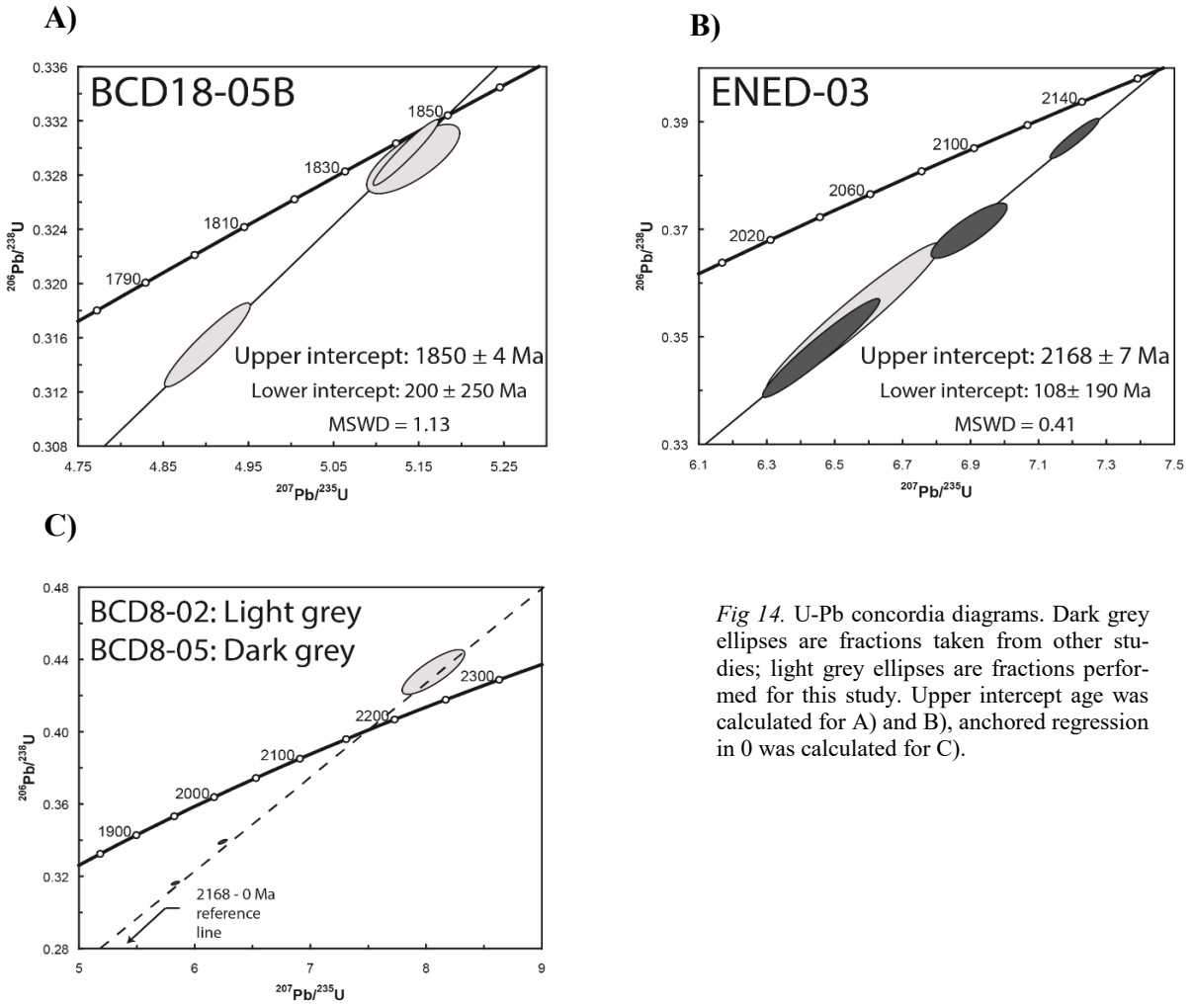

Fig 14. U-Pb concordia diagrams. Dark grey ellipses are fractions taken from other studies; light grey ellipses are fractions performed for this study. Upper intercept age was calculated for A) and B), anchored regression in 0 was calculated for C).

5 Results

5.1 Geochronology

U-Pb TIMS measurements are reported in Table 1 and age results are shown in concordia diagrams in Figure 14.

5.1.1 BCD18-05B

Three fractions with moderately brown baddeleyite grains were analyzed (Fig. 14-A). The Bd-b and Bd-c fractions overlap and plot slightly below the concordia, at 0.6 % and 1.1% respectively. The Bd-a fraction plots discordant by 4.2 %. Regression yields upper and lower intercepts at 1850 ± 4 and 200 ± 250 Ma, respectively (MSWD = 1.13). The upper intercept of 1850 ± 4 Ma is interpreted as the crystallization age for this sample.

5.1.2 ENED-03

Three fractions of the ENED-03 dyke were analyzed by Larsson (2015) and therefore only one additional fraction was prepared for this study. Fraction Bd-mff2, comprising three small moderately brown baddeleyite grains plot as much as 9.6% discordant. Combining analysis of this fraction and the fractions measured by Larsson (2015) give upper and lower intercepts at 2168 ± 7 and 108 ± 190 Ma respectively (MSWD = 0.41). The upper intercept age is interpreted as the crystallization age of the dyke (Fig. 13-B).

5.1.3 ENED-03S

Some attempts to date the ENED-03S sill were performed. However only few tiny baddeleyite-alike grains were recovered, the cleaning and dating process on these was not successful.

5.1.4 BCD8-02

One fraction of a single small light brown baddeleyite grain was analyzed and regressed together with two unpublished analyses that were obtained by Johan Olsson in Toronto 2008 (Fig. 14-C). The Bd-a fraction plots slightly reversed discordant (0.70%), i.e. slightly above the Concordia curve. Regression using an anchored lower intercept at 0 Ma yields an upper intercept age at ca. ~2168 Ma. This is identical with the $^{207}Pb/^{206}Pb$ date of fraction Bd-a at 2166 ± 27 Ma. The upper intercept at 2168 Ma is interpreted as the crystallization age BCD8-02.

5.2 Geochemistry

Major and trace element analyses are presented in Table 2, and geochemical data of the studied samples are shown in Figs 15 - 17. In the total alkali-silica (TAS) diagram (LeBas et al. 1986; Fig. 15) all samples plot in the sub-alkaline field and, most of them display basaltic composition except the BCD8-02 dyke which plots in the andesitic field.

Sample		ENED-03	ENED-03R	ENED-03S	BCD8-02	BCD18-05B
Major Oxides (%)	SiO2	48.75	49.4	50.1	53.24	49.20
	Al2O3	13.89	14.6	14.1	8.32	12.40
	Fe2O3	13.36	13.4	13.4	12.32	18.20
	CaO	10.33	9.63	11.8	11.16	8.77
	MgO	7.17	6.47	7.04	9.16	4.80
	Na2O	2.00	2.72	2.13	1.64	2.25
	K2O	0.66	0.95	0.29	0.85	0.91
	MnO	0.20	0.21	0.22	0.19	0.24
	TiO2	1.04	1.15	1.07	0.94	2.65
	P2O5	0.09	0.11	0.1	0.09	0.32
	Cr2O3	0.033	0.03	0.04	0.070	0.01
	LOI	2.2	1.74	0.01	1.7	0.28
	SO3	0	0.356	0.032	0	0.272
	Total	99.723	100.766	100.332	99.68	100.302
Trace Elements (ppm)	Ba	145	153	68	283	243
	Be	<1	<1	<1	3	3
	Co	67.0	53.2	47.9	66.8	92.7
	Cs	1.8	1.3	0.7	0.4	4.7
	Ga	15.3	15.3	14.5	10.1	21.9
	Hf	2.7	2.9	1.9	3.4	6.1
	Nb	5.2	5.5	2.1	7.4	18.2
	Rb	31.4	47.2	6.3	24.0	36.2
	Sn	<1	<1	<1	<1	3
	Sr	153.5	188.8	124.5	118.5	129.1
	Ta	0.3	0.4	0.2	0.7	1.0
	Th	1.7	1.6	0.5	6.3	5.7
	U	0.4	0.4	0.1	1.9	1.4
	V	222	214	315	267	476
	W	125.2	<0.5	<0.5	134.7	352.8
	Zr	102.5	106.9	61.6	127.6	242.5
	Y	26.8	25.4	23.2	24.6	51.2
	La	11.7	12.1	4.4	21.2	25.5
	Ce	25.0	24.2	10	42.2	55.2
	Pr	3.00	3.07	1.49	4.87	7.50
	Nd	13.8	13.7	7.5	19.7	31.4
	Sm	3.43	3.44	2.46	4.33	7.85
	Eu	1.10	1.09	0.91	1.14	2.28
	Gd	4.20	3.88	3.33	4.71	9.46
	Tb	0.73	0.7	0.61	0.76	1.56
	Dy	4.53	4.62	4.29	4.70	9.42
	Ho	0.92	0.95	0.9	0.97	2.05
	Er	3.00	3.02	2.62	2.66	5.91
	Tm	0.39	0.42	0.38	0.36	0.85
	Yb	2.78	2.77	2.42	2.30	5.48
	Lu	0.41	0.42	0.37	0.35	0.83
	Mo	-	0.4	0.2	-	0.5
	Cu	-	76.7	161.4	-	284.1
	Pb	-	1.8	0.6	-	4.5
	Zn	-	45	35	-	72
	Ni	64	30.9	22.8	172	29.0
	As	-	<0.5	<0.5	-	<0.5
	Cd	-	<0.1	<0.1	-	0.1
	Sb	-	<0.1	<0.1	-	<0.1
	Bi	-	<0.1	<0.1	-	<0.1
	Ag	-	<0.1	<0.1	-	<0.1
	Au	-	<0.5	2.4	-	6.3
	Hg	-	<0.01	<0.01	-	<0.01
	Tl	-	<0.1	<0.1	-	0.2
	Se	-	<0.5	<0.5	-	<0.5
	Sc	39	-	-	35	-

Table 2. Major oxides and trace element analyses on mafic dykes and a sill from the Transvaal Supergroup.

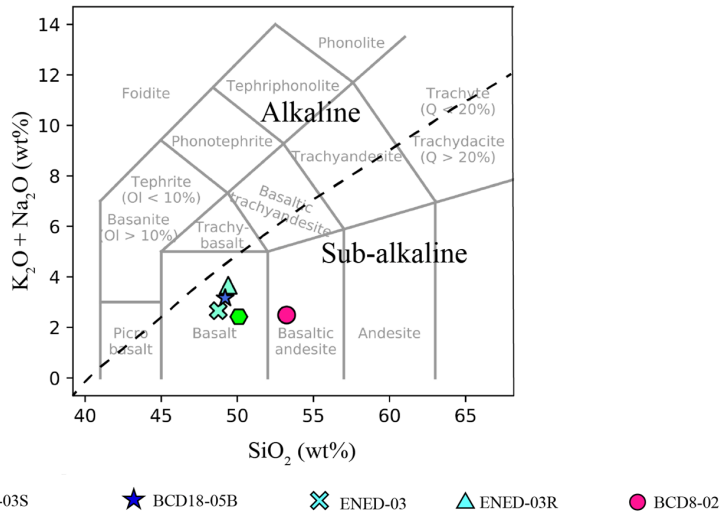

Fig 15. TAS diagram after LeBas et al. (1986) with the studied samples. The dashed line represents the division of the alkaline and sub-alkaline magmatic series.

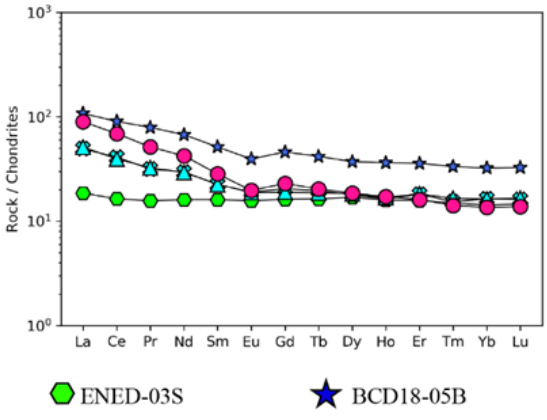

Fig 16. REE diagrams with the studied samples normalized to chondrite after Sun& McDonough (1989).

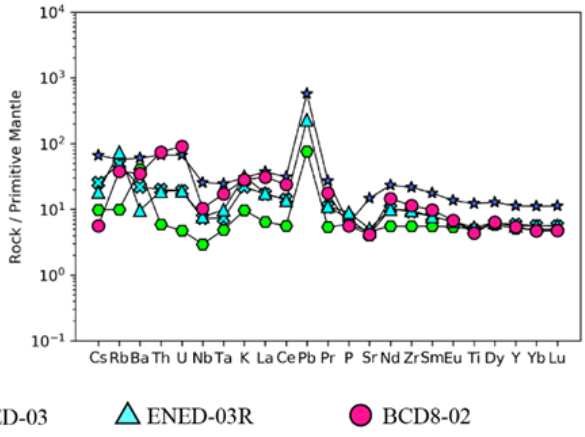

Fig 17. Multi-element diagrams with the studied samples normalized to primitive mantle after Sun& McDonough (1989).

The rare earth elements (REE) normalization diagram to chondrite (McDonough & Sun 1995; Fig. 16) displays a similar pattern for BCD8-02, ENED-03/ ENED-03R and BCD18-05. These samples show enriched but decreasing light REE (LREE), with a minor negative anomaly in Eu, and a flat trend in heavy REE (HREE). The sill ENED-03S displays a flat REE trend. In the multi-element normalization diagram to pyrolite mantle (McDonough & Sun 1995; Fig. 17), all samples have similar patterns, although with some contrasting anomalies. In the large ion lithophile (LIL) elements, the samples show a positive anomaly for Rb and a negative anomaly for Ba, excluding ENED-03S sill, which has increases from Rb to Ba. The high field strength (HFS) elements; including Th and U, also plot differently. Dyke ENED-03/ENED-03R displays a flat profile, the ENED-03S sill has a negative slope, whereas BCD8-02 and BCD18-05B have a positive slope. All the samples show a negative anomaly in Nb, and a slight increase in Ta, coupled with Nb. Positive anomalies in K and Pb are common for all samples, with negative anomalies in P and Sr, excluding the BCD18-05B dyke which shows a slight increase. The most compatible HFS elements show a relatively flat and constant trend, with a minor negative Ti anomaly.

6 Discussion

6.1 U-Pb data interpretation

The ID-TIMS U-Pb geochronology performed on baddeleyite from BCD18-05B and ENED-03 yield upper intercept dates of 1850 ± 4 and 2168 ± 7 Ma, respectively, based on regression of analyses that plot slightly to moderately discordant (Fig. 14). MSWD values of 1.13 and 0.41 for these samples, suggest the upper intercept dates are statistically reliable and are thus interpreted as crystallization ages. The $^{207}Pb/^{206}Pb$

date of the single fraction of BCD8-02 dyke is 2166 ± 27 Ma, and plots slightly above the concordia. As can be seen in Figure 14, this fraction and the two analyses of sample BCD8-05 (obtained by Johan Olsson during his visit at Jack Satterly Laboratory, at the Toronto University in Canada) all fall on, or just aside, a 2168 Ma discordia line. Despite having no definite crystallization ages for these dykes, they are interpreted to belong to the ca. 2168 Ma event of mafic magmatism.

The lower intercept dates for the BCD18-05B and ENED-03 dykes at 200 ± 250 and 108 ± 190 Ma, respectively, indicate a possible post-magmatic event that caused moderate disturbance of the U-Pb isotopic system (Fig. 14). However, baddeleyite grains do not show any distinct signs of alteration such as rims or frosty crystal surfaces, which is typically seen in baddeleyite that have reacted with silica to form secondary zircon. However, petrographic studies of thin sections (see Figs. 6-7, 9-10 and 12-13) reveal that these rocks have experienced alteration and fluid activity, in contrast to the structurally younger sill in the KwaZulu Natal area (samples ENED-03S/-SN). This sill, assumed to belong to the Karoo magmatic event, has a pristine mineralogy, as is typical for intrusions of the Karoo event. The widespread Karoo magmatism may have caused alteration and isotopic disturbance of baddeleyite in older mafic intrusions, and as shown in Figure 4, Karoo igneous rocks are widespread in the sample area.

6.2 Timing and geochemistry of the Mashining event

Before this study, the age of the Mashining event was constrained by two amphibole $^{40}Ar/^{39}Ar$ plateau ages of 2253 ± 45 and 2202 ± 74 Ma (Wabo et al. 2019). These age results are important as they identify the Mashining event as a separate dyking event, significantly older than the 1875 – 1835 Ma Black Hills dykes further north (Fig. 22). The new and more precise U-Pb baddeleyite ages for the BCD18-05B dyke and BCD8-02 dyke (the latter being the same dyke as the LDB sample in Wabo; et al. (2019) yielding the $^{40}Ar/^{39}Ar$ age of 2253 ± 45 and 2202 ± 74 Ma) suggest that the true age of these dykes is ca. 2168 Ma (Fig. 14).

The geochemical data agrees with the interpretation that the BCD8-02 dyke is part of the Mashining dyke swarm and together with published geochemical data (Wabo et al. 2019) help to define a geochemical signature for the magmatic rocks of the Mashining event. The REE signature of the BCD8-02 dyke displays an enriched LREE trend and flat HREE trend similar to the Mashining data (Wabo et al. 2019; Fig. 18-A). In the multi-element diagrams (Fig. 19-A), dyke BCD8-02 displays positive anomalies for LIL incompatible elements (e.g., Rb, Ba and K) and have negative anomalies at HFS elements (e.g. Nb, Ta and Ti), similar to the Mashining data-set with the exception of the negative K anomaly, which is attributed to metasomatism alteration (Wabo et al. 2019).

The newly defined Mashining dyke swarm is compared with geochemical data of coeval (i.e. referred as a similar age range) magmatic events, which are the Hekpoort and Machadodorp. The Mashining dyke swarm seems to be related to the Hekpoort magmatism. Both have similarities in regards of age range, REE signature, trace element anomalies and element ratios (Fig. 18 - 21). In these, the latter of both sets plot towards arc-related basalts (Fig. 20) and above the OIB-MORB array (Fig. 21), indicating interaction of a common magma source with a crustal component, which is further supported by the positive Rb, Th, U and negative Nb-Ta, as well as Ti anomalies (Fig. 19; Ernst 2014).

The 2168 ± 7 Ma dyke ENED-03/-03R is located much further to the south (Fig. 22). Its crystallization age together with another dyke age at ca. 2165 Ma (Ashley Gumsley, personal communication) make them part of the Mashining event, despite the distance from the Mashining swarm, and the geochemical differences with the similarly magmatic units, i.e., the Hekpoort and Mashining, the age is weighted in the interpretation (Figs. 18 and 19). The REE signature of the ENED-03 dyke, the multi-element and element ratio diagrams resembles that of the Black Hills swarm (Figs. 18-C and 19-F), but their relationship is unlikely given the 300 Myr age difference and spatial separation up to 300 km. This dyke, therefore, might be part of a coeval ENE-trending dyke swarm in the area of the White Mfolozi river (Fig. 4). The extent and distribution of ca. 2168 Ma dykes in this area is uncertain since previous work reveal the existence of many dykes of different generation and trends occur in this part of the craton (Gumsley et al. 2013; Larsson 2015; Gumsley et al. 2016).

6.3 Timing and geochemistry of the Black Hills event

The age of the Black Hills Dyke swarm spans ca. 40 Myr, between 1875 Ma and 1835 Ma. Olsson et al. (2016) performed dating on dykes of this swarm, especially the NNE- to NE trending dykes in the area near the Transvaal sub-basin of the Transvaal Supergroup. Olsson et al. (2016) divided the swarm into two subsets, one slightly older more primitive subset (1875 – 1856 Ma) with high MgO content (6.8 – 9.4%) and one younger, more differentiated subset (1859 – 1832 Ma) with lower MgO content (4.2 – 5.6%). Dyke

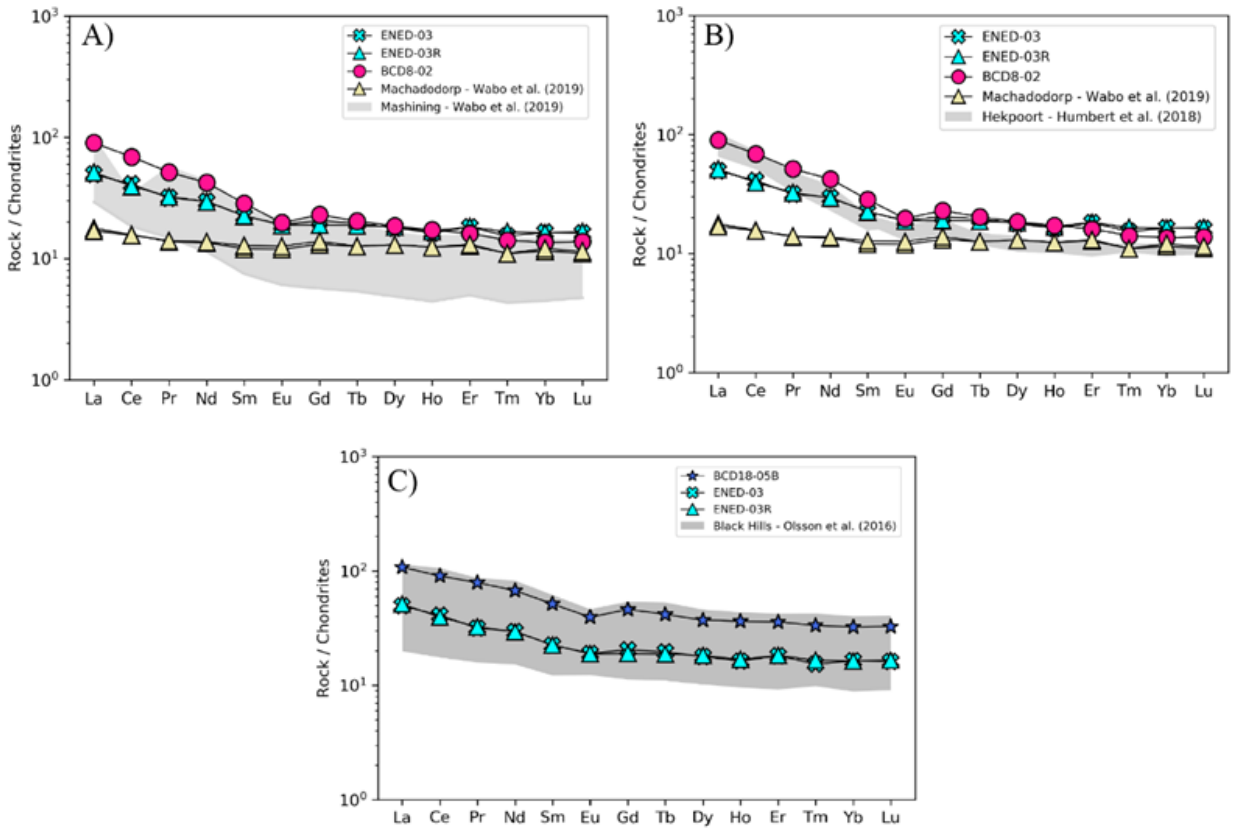

Fig. 18. REE diagrams comparing BCD8-02 and ENED-03/ENED-03R dykes against Mashining (Wabo et al. 2019), Hekpoort (Humbert et al. 2018) and Machadodorp and data-sets (A and B). REE diagram comparing BCD18-05B and ENED-03/ENED-03R dykes against Black Hills (Olsson et al. 2016) data-set (C). Samples are normalized to chondrite after Sun& McDonough (1989).

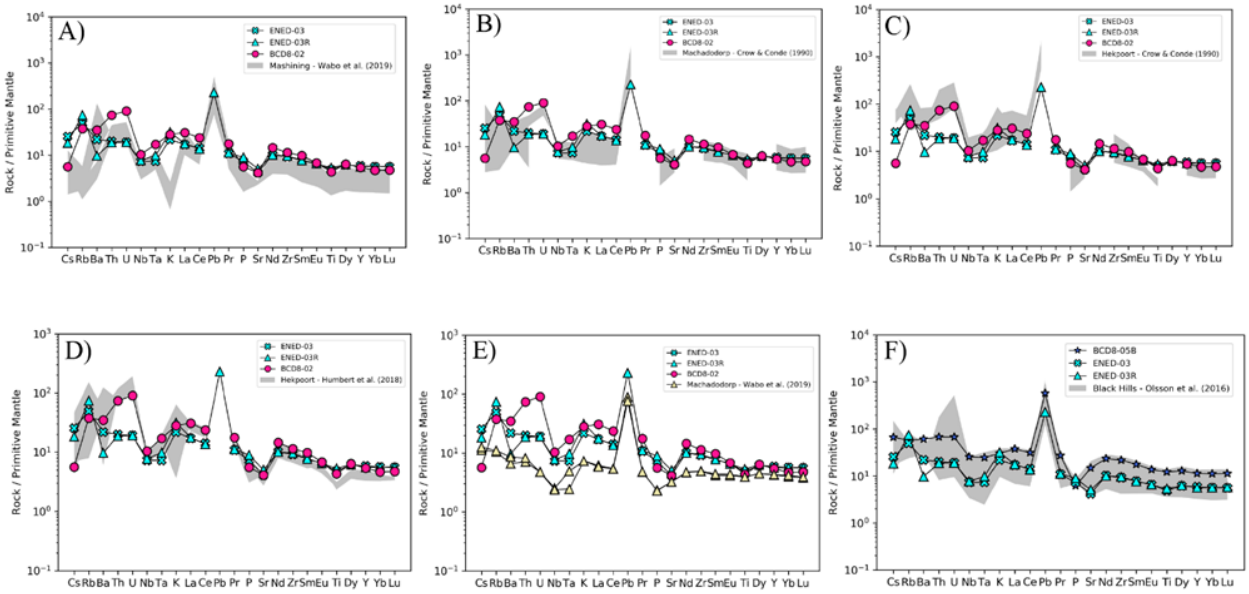

Fig 19. Multi-element diagrams comparing BCD8-02 and ENED-03/ENED-03R dykes against Mashining (Wabo et al. 2019), Hekpoort (Crow & Condie 1990; Humbert et al. 2018) and Machadodorp (Crow & Condie 1990; Wabo et al. 2019) data-sets (A-E). Multi-element diagram comparing BCD18-05B and ENED-03/ENED-03R dykes against Black Hills (Olsson et al. 2016) data-set (F). Samples are normalized to chondrite after Sun& McDonough (1989).

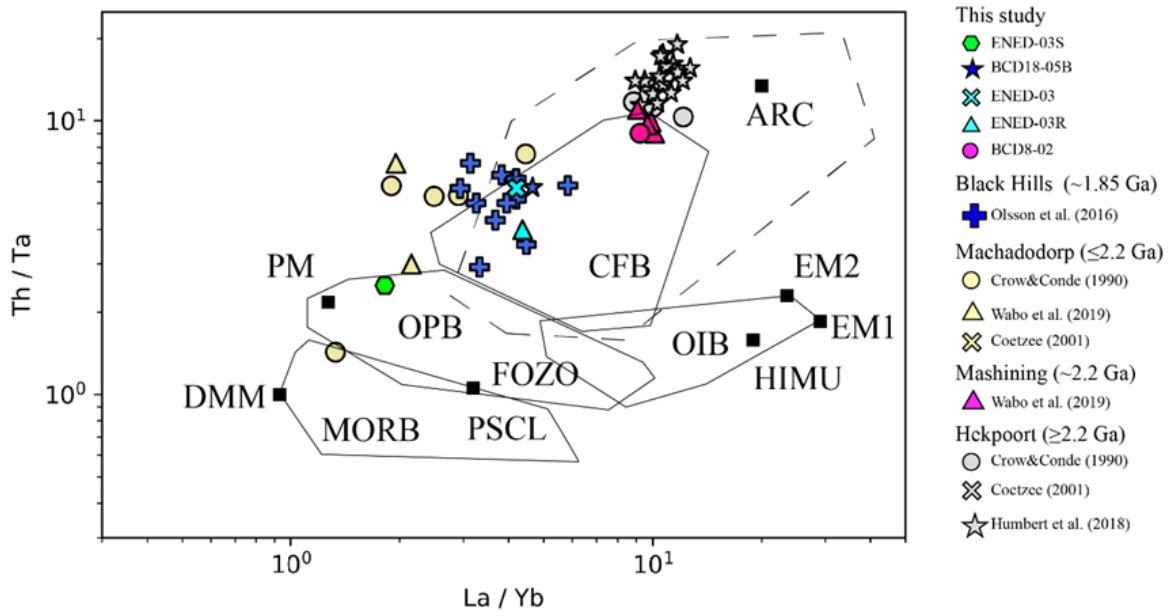

Fig. 20. REE diagrams comparing BCD8-02 and ENED-03/ENED-03R dykes against Mashining (Wabo et al. 2019), Hekpoort (Humbert et al. 2018) and Machadodorp and data-sets (A and B). REE diagram comparing BCD18-05B and ENED-03/ ENED-03R dykes against Black Hills (Olsson et al. 2016) data-set (C). Samples are normalized to chondrite after Sun& McDonough (1989).

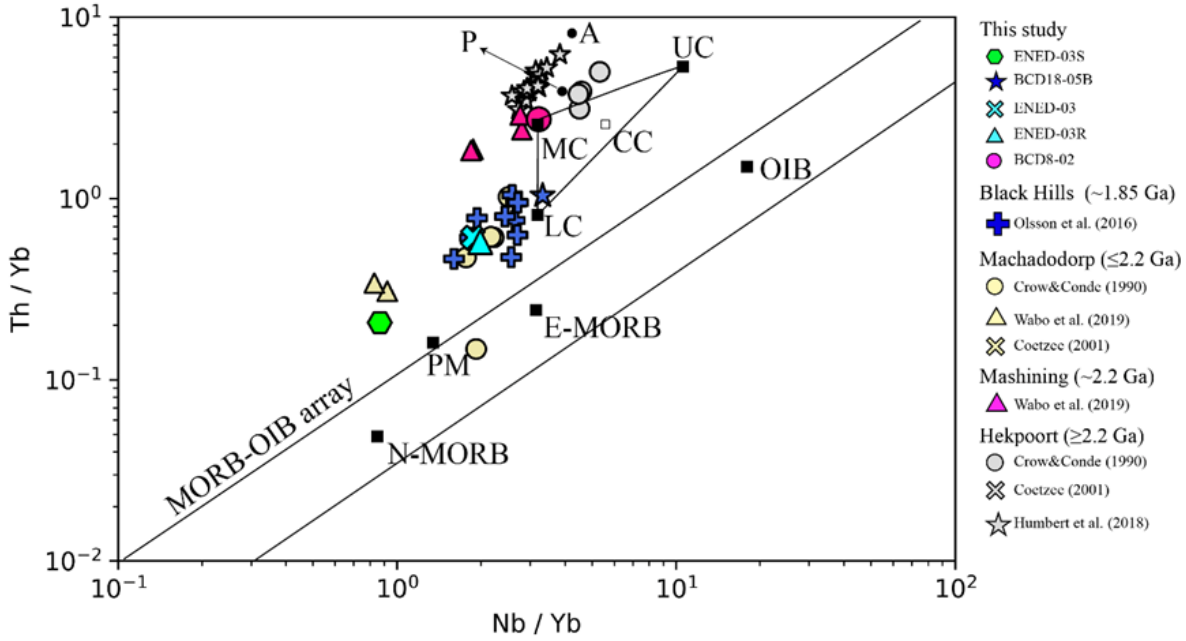

Fig. 21. REE diagrams comparing BCD8-02 and ENED-03/ENED-03R dykes against Mashining (Wabo et al. 2019), Hekpoort (Humbert et al. 2018) and Machadodorp and data-sets (A and B). REE diagram comparing BCD18-05B and ENED-03/ENED-03R dykes against Black Hills (Olsson et al. 2016) data-set (C). Samples are normalized to chondrite after Sun& McDonough (1989).

BCD18-05 yields an upper intercept age at 1850 ± 7 Ma (Fig. 14-a), which makes it part of the younger, more evolved (low MgO) subset of Black Hills dykes. Klausen et al. (2010) inferred a LIP origin for the Black Hills dykes, whereas Olsson et al. (2016) favored a back-arc setting as part of amalgamation of the Columbia supercontinent.

Geochemical data of the BCD18-05B dyke agrees with the typical geochemical signature of the younger subset (1859 – 1832 Ma) of the Black Hills dyke swarm. In a REE diagram (Fig. 18-C), the dyke displays the same signature to the Black Hills dykes, which has higher REE content in comparison with the other studied units (i.e., Hekpoort and Mashining). Multi-element diagrams (Fig. 19-F), also shows simi-

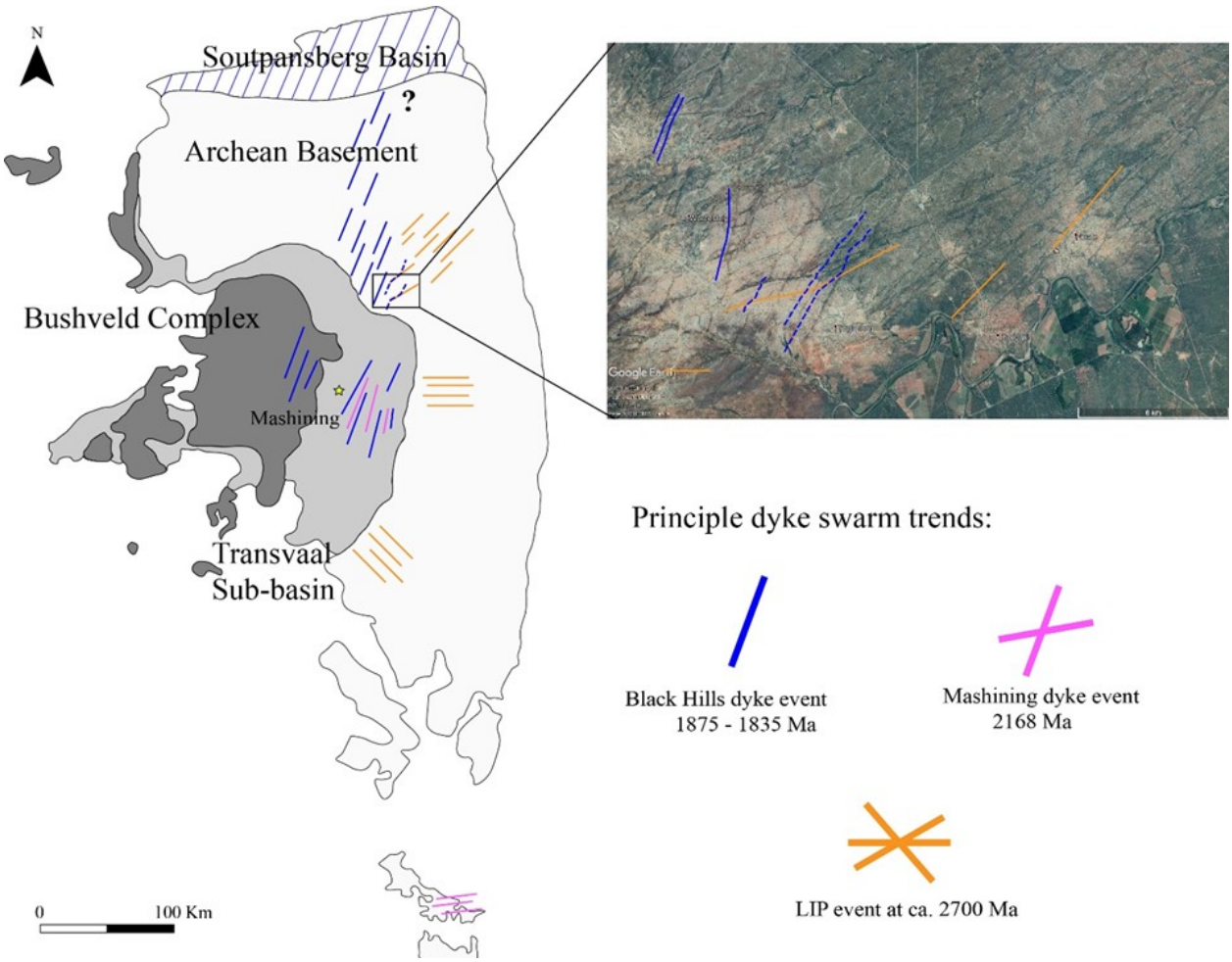

Fig. 22. Simplified map of the eastern margin of the Kaapvaal Craton showing the different dyke events in the area. The blue lines represent the Black Hills event (1875 – 1835 Ma), the pink Mashining event and the orange the ca. 2.70 Ga event. Note the transition in the trend from the Black Hills swarm from an NNE trend in the Transvaal Sub-basin to an NE trend in the Archean Basement. The most southern dykes are classified as Mashining dykes based on their age despite not showing similar geochemical signature. Modified after Olsson et al. (2016).

larities in certain anomalies, such as the positive anomalies in Th, U and Pb and the negative anomalies in Nb, Ta and P. These anomalies likely indicate magma contamination by continental crust or a subduction setting (Ernst 2014), which is confirmed in the element ratio diagrams (Figs. 20 and 21), where the BCD18-05B dyke plots together with the Black Hills dyke swarm in the fields of continental flood basalts and arc -related basalts. In the La/Yb vs Th/Ta diagram (Fig. 21) the data plots above the mantle array indicating a crustal component in the magma source, particularly from the lower crust.

6.4 New definition of dyke swarms in eastern Kaapvaal Craton

In Figure 22, the spatial distribution of the main dyke events in the eastern Kaapvaal Craton are tentatively illustrated. Olsson et al. (2011) describes a LIP event at ca. 2.7 Ga composed by three radiating set of dykes, which from south to north are: the Badplaas-Barberton (SE–trending and intermixed with ca. 2.97-2.96 Ga dykes), ca. 2.70-2.66 Ga Rykoppies (E – trending), and the 2.70-2.66 Ga NE-trending set. The Mashining event is defined as a ca. 2168 Ma swarm of dioritic-doleritic NNE-trending dykes with an estimated dyke width of 40 km. As shown in Figure 22, the Black Hills swarm spreads across a relatively extensive area, intruding into the Bushveld Complex, the Transvaal Supergroup and the Archean Basement farthest to the east, and seems, at least in the south, intermixed with the older Mashining dykes.

From the occurrences and distribution of the Mashining and the Black Hills dykes, the Black Hills dykes can be inferred to follow a trend controlled by former regional stresses that define the trend of former dyke events (Ernst et al. 1995; Hou et al. 2010; Ernst 2014). Note that in the area near the Transvaal Supergroup, the younger 1.88 – 1.83 Ga Black Hills dykes seem deflected in an echelon pattern, following the

trend of the 2.7 Ga dykes, as shown in the Google Earth inset map of Figure 22. This pattern is interpreted as secondary deformation causing an offset in the orientation of the swarm (Ernst et al. 1995; Ernst 2014). Further south, the Black Hills dykes follow the same NNE-trend as the ca. 2168 Ma Mashining dykes. Finally, the trend and extension of the Black Hills swarm, which spans to the north close to the ca. 1.85 Ga Soutpansberg Group basin (Cheney et al. 1990; Fig. 22) seems to suggest a likely connection of the swarm as feeder of the mafic volcanic rocks found in the basin.

6.5 Potential global correlations

The definition of the ca. 2168 Ma Mashining dyke event in the Kaapvaal Craton leads to the possibility of linking the Kaapvaal Craton to other cratons, that host mafic intrusions of the same age. For instance, a Superior – Wyoming connection can be suggested based on paleomagnetic and geochronological studies of the ca. 2170 Ma Biscotasing and Payne river dyke swarms in the Superior Craton, with doleritic dykes in the Wind River area from Wyoming Craton (Ernst & Bleeker 2010). Another important event dated at ca. 2170 Ma is the Dandeli and Bandepalem dyke swarms in the Dharwar Craton (French & Heaman 2010; Srivastava et al. 2019).

7 Conclusions

- The emplacement age of the Mashining dyke swarm is here revised to ca. 2168 Ma, i.e. some tens of Myr younger than indicated from recently published $^{40}Ar/^{39}Ar$ dates (Wabo et al. 2019). A major portion of Mashining dykes occur in the lower Transvaal Supergroup in the Mpumalanga area. The Mashining dyke swarm is intermixed with the younger, but similar trending, dykes of the 1875-1835 Ma Black Hills swarm.

- Towards the north, the NNE-trending Black Hills dyke swarm intersects a major NE-trending dyke swarm, comprising ca. 2.7 Ga dykes. In this intersecting area, within the Archaean basement just east of the Transvaal Supergroup, the Black Hills dykes form an echelon pattern which is readily visible from Google Earth images. It thus seems likely that second deformation affected the trend of the Black Hills swarm and the NE-trending ca. 2.70 Ga dykes, whereas within the basin, the Black Hills dykes may have followed the NNE trend of ca. 2168 Ma dykes of the Mashining swarm.

- The new interpretation of the original trend and extension of the Black Hills dykes swarm suggest these could be feeder dykes of the mafic volcanic rocks within the Soutpansberg Basin further north.

- Geochronological and geochemical data suggest a direct link between the ca. 2168 Ma dykes of the Mashining swarm and Hekpoort magmatism, such that the former acted as feeder dykes of the Hekpoort volcanic units within the Pretoria Group of the Transvaal Supergroup. The Mashining dykes display similar geochemical REE signatures and trace element ratios as the Hekpoort volcanic rocks.

- The ca. 2168 Ma age of the ENED-03 dyke represents a southern extension of the Mashining magmatism. However, there are considerable geochemical differences that require further studies.

- The ca. 2168 Ma age of the Mashining event indicate a possible link to coeval magmatic events on a global scale. Intrusions of this age occur for instance in the Wyoming, Dharwar and Superior cratons.

8 Acknowledgments

I would like to thank to my supervisor Ulf Söderlund and co-supervisor Ashley Gumsley for their tireless support and help throughout this project. We all know it was full of challenges (i.e. bad luck at the early stage - not all the diabase dyke contain baddeleyite), but also many great learning and good times. I would like to thank also to my family and friends for their support and encouragement, specially thanks to Cata for being an unconditional support not only on this project but in the master in general.

9 References

Bleeker, W., 2004: Taking the pulse of planet Earth: a proposal for a new multi-disciplinary flagship project in Canadian solid Earth sciences. *J Geoscience Canada 31*.

Bleeker, W. & Ernst, R., 2006: Short-lived mantle generated magmatic events and their dyke swarms: the key unlocking Earth's paleogeographic record back to 2.6 Ga. *Dyke swarms–time markers of crustal evolution*, 3-26.

Bryan, S. E. & Ernst, R. E., 2008: Revised definition of large igneous provinces (LIPs). *Earth-Science Reviews 86*, 175-202.

Buick, I. S., Maas, R. & Gibson, R., 2001: Precise U–Pb titanite age constraints on the emplace-

ment of the Bushveld Complex, South Africa. *journal of geological society 158*, 3-6.
Catuneanu, O. & Eriksson, P. G., 2002: Sequence stratigraphy of the Precambrian Rooihoogte–Timeball Hill rift succession, Transvaal Basin, South Africa. *Sedimentary Geology 147*, 71-88.
Cawthorn, R. G. 2015: The Bushveld Complex, South Africa. *In Layered Intrusions*, 517-587. Springer,
Cederberg, J., Söderlund, U., Oliveira, E. P., Ernst, R. E. & Pisarevsky, S. A., 2016: U-Pb baddeleyite dating of the Proterozoic Pará de Minas dyke swarm in the São Francisco craton (Brazil)–implications for tectonic correlation with the Siberian, Congo and North China cratons. *Gff 138*, 219-240.
Cheney, E., Barton, J. & Brandl, G., 1990: Extent and age of the Soutpansberg sequences of southern Africa. *South African Journal of Geology 93*, 664-675.
Coetzee, L., Beukes, N., Gutzmer, J. & Kakegawa, T., 2006: Links of organic carbon cycling and burial to depositional depth gradients and establishment of a snowball Earth at 2.3 Ga. Evidence from the Timeball Hill Formation, Transvaal Supergroup, South Africa. *South African Journal of Geology 109*, 109-122.
Coetzee, L. L., 2001: *Genetic stratigraphy of the Paleoproterozoic Pretoria Group in the Western Transvaal*. Rand Afrikaans University. 220 pp.
Condie, K. C., 2003: Incompatible element ratios in oceanic basalts and komatiites: tracking deep mantle sources and continental growth rates with time. *Geochemistry, Geophysics, Geosystems 4*, 1-28.
Cornell, D., Schütte, S. & Eglington, B., 1996: The Ongeluk basaltic andesite formation in Griqualand West, South Africa: submarine alteration in a 2222 Ma Proterozoic sea. *Precambrian Research 79*, 101-123.
Crow, C. & Condie, K. C., 1990: Geochemistry and origin of early Proterozoic volcanic rocks from the Transvaal and Soutpansberg successions, South Africa. *Precambrian Research 47*, 17-26.
Dorland, H. C., 2004: *Provenance ages and timing of sedimentation of selected Neoarchean and Paleoproterozoic successions on the Kaapvaal Craton*. University of Johannesburg.
Emst, R. E. & Buchan, K. L., 2001: The use of mafic dike swarms in identifying and locating mantle plumes. *Geological Societ of America Special Paper 352*, 247.
Eriksson, P. G., Altermann, W. & Hartzer, F. J. 2006: The Transvaal Supergroup and its precursors. *In Geology of South Africa*, 237-260. Geological Society of South Africa,
Ernst, R. & Bleeker, W. J. C. J. O. E. S., 2010: Large igneous provinces (LIPs), giant dyke swarms, and mantle plumes: significance for breakup events within Canada and adjacent regions from 2.5 Ga to the Present. *47*, 695-739.
Ernst, R., Buchan, K. & Palmer, H., 1995: Giant dyke swarms: characteristics, distribution and geotectonic applications. *Physics and Chemistry of dykes*, 3-21.
Ernst, R. E., 2014: *Large igneous provinces*. Cambridge University Press.
Ernst, R. E., Bleeker, W., Söderlund, U. & Kerr, A. C., 2013: Large Igneous Provinces and supercontinents: Toward completing the plate tectonic revolution. *Lithos 174*, 1-14. doi: 10.1016/j.lithos.2013.02.017
French, J. E. & Heaman, L. M., 2010: Precise U–Pb dating of Paleoproterozoic mafic dyke swarms of the Dharwar craton, India: Implications for the existence of the Neoarchean supercraton Sclavia. *Precambrian Research 183*, 416-441. doi: 10.1016/j.precamres.2010.05.003
Frick, C., 1988: 1:250 000 Geological series - 2830 Dundee. South Africa, Department of mineral and energy affairs.
Gumsley, A., Rådman, J., Söderlund, U. & Klausen, M., 2016: U–Pb baddeleyite geochronology and geochemistry of the White Mfolozi Dyke Swarm: Unravelling the complexities of 2.70 –2.66 Ga dyke swarms across the eastern Kaapvaal Craton, South Africa. *Gff 138*, 115-132.
Gumsley, A. P., Chamberlain, K. R., Bleeker, W., Soderlund, U., De Kock, M. O., Larsson, E. R. & Bekker, A., 2017: Timing and tempo of the Great Oxidation Event. *Proc Natl Acad Sci U S A 114*, 1811-1816. doi: 10.1073/pnas.1608824114
Gumsley, A. P., De Kock, M. O., Rajesh, H. M., Knoper, M. W., Söderlund, U. & Ernst, R. E., 2013: The Hlagothi Complex: The identification of fragments from a Mesoarchaean large igneous province on the Kaapvaal Craton. *Lithos 174*, 333-348. doi: 10.1016/j.lithos.2012.06.007
Hannah, J. L., Bekker, A., Stein, H. J., Markey, R. J. & Holland, H. D., 2004: Primitive Os and 2316 Ma age for marine shale: implications for Paleoproterozoic glacial events and the rise of atmospheric oxygen. *Earth Planetary Science Letters 225*, 43-52.
Hou, G., Kusky, T., Wang, C. & Wang, Y., 2010: Mechanics of the giant radiating Mackenzie dyke swarm: a paleostress field modeling. *Journal of Geophysical Research: Solid Earth 115*.
Humbert, F., De Kock, M. O., Altermann, W., Elburg, M. A., Lenhardt, N., Smith, A. J. B. & Masango, S., 2018: Petrology, physical volcanology and geochemistry of a Paleoproterozoic large igneous province: The Hekpoort Formation in the southern Transvaal subbasin (Kaapvaal craton). *Precambrian Research 315*, 232-256. doi: 10.1016/j.precamres.2018.07.022
Irvine, T. & Baragar, W., 1971: A guide to the chemical classification of the common volcanic rocks. *J Canadian journal of earth sciences 8*, 523-548.

Klausen, M. B., Söderlund, U., Olsson, J. R., Ernst, R. E., Armoogam, M., Mkhize, S. W. & Petzer, G., 2010: Petrological discrimination among Precambrian dyke swarms: Eastern Kaapvaal craton (South Africa). *Precambrian Research 183*, 501-522. doi: 10.1016/j.precamres.2010.01.013

Larsson, E., 2015: *U-Pb baddeleyite dating of intrusions in the south-easternmost Kaapvaal Craton (South Africa): revealing multiple events of dyke emplacement*. Lund, Sweden, Lund University.

Lebas, M. J., Maitre, R. L., Streckeisen, A. & Zanettin, B., 1986: A chemical classification of volcanic rocks based on the total alkali-silica diagram. *Journal of Petrology 27*, 745-750.

Lenhardt, N., Eriksson, P. G., Catuneanu, O. & Bumby, A. J., 2012: Nature of and controls on volcanism in the ca. 2.32–2.06Ga Pretoria Group, Transvaal Supergroup, Kaapvaal Craton, South Africa. *Precambrian Research 214-215*, 106-123. doi: 10.1016/j.precamres.2011.09.012

Lubnina, N., Ernst, R., Klausen, M. & Söderlund, U., 2010: Paleomagnetic study of NeoArchean–Paleoproterozoic dykes in the Kaapvaal Craton. *Precambrian Research 183*, 523-552. doi: 10.1016/j.precamres.2010.05.005

Ludwig, K. R., 2003: Isoplot 3.00: A geochronological toolkit for Microsoft Excel. J Berkeley Geochronology Center Special Publication. 70 pp.

Luo, G., Ono, S., Beukes, N. J., Wang, D. T., Xie, S. & Summons, R. E., 2016: Rapid oxygenation of Earth's atmosphere 2.33 billion years ago. *Science Advances 2*. doi: 10.1126/sciadv.1600134

Mcdonough, W. F. & Sun, S.-S., 1995: The composition of the Earth. *Chemical Geology 120*, 223-253.

Oberholzer, J. D. & Eriksson, P. G., 2000: Subaerial volcanism in the Palaeoproterozoic Hekpoort Formation (Transvaal Supergroup), Kaapvaal craton. *Precambrian Research 101*, 193-210.

Olsson, J. R., Klausen, M. B., Hamilton, M. A., März, N., Söderlund, U. & Roberts, R. J., 2016: Baddeleyite U–Pb ages and gechemistry of the 1875–1835 Ma Black Hills Dyke Swarm across north-eastern South Africa: part of a trans-Kalahari Craton back-arc setting? *Gff 138*, 183-202. doi: 10.1080/11035897.2015.1103781

Olsson, J. R., Söderlund, U., Hamilton, M. A., Klausen, M. B. & Helffrich, G. R. J. N. G., 2011: A late Archaean radiating dyke swarm as possible clue to the origin of the Bushveld Complex. *Nature Geoscience 4*, 865.

Olsson, J. R., Söderlund, U., Klausen, M. B. & Ernst, R. E., 2010: U–Pb baddeleyite ages linking major Archean dyke swarms to volcanic-rift forming events in the Kaapvaal craton (South Africa), and a precise age for the Bushveld Complex. *Precambrian Research 183*, 490-500. doi: 10.1016/j.precamres.2010.07.009

Pearce, J. A., 2008: Geochemical fingerprinting of oceanic basalts with applications to ophiolite classification and the search for Archean oceanic crust. *Lithos 100*, 14-48.

Rasmussen, B., Bekker, A. & Fletcher, I. R., 2013: Correlation of Paleoproterozoic glaciations based on U–Pb zircon ages for tuff beds in the Transvaal and Huronian Supergroups. *Earth Planetary Science Letters 382*, 173-180.

Reczko, B., Oberholzer, J., Res, M., Eriksson, P. & Schreiber, U., 1995: A re-evaluation of the volcanism of the Palaeoproterozoic Pretoria Group (Kaapvaal craton) and a hypothesis on basin development. *Journal of African Earth Sciences 21*, 505-519.

Schröder, S., Beukes, N. J. & Armstrong, R. A., 2016: Detrital zircon constraints on the tectonostratigraphy of the Paleoproterozoic Pretoria Group, South Africa. *Precambrian Research 278*, 362-393.

Schröder, S. & Warke, M. R., 2016: Termination of BIF deposition in the Paleoproterozoic: the Tongwane Formation, South Africa. *South African Journal of Geology 119*, 329-346.

Smit, P. J., 1986: 1:250 000 Geological series - 2530 Barberton. South Africa, Department of mineral and energy affairs.

Söderlund, U. & Johansson, L., 2002: A simple way to extract baddeleyite (ZrO2). *Geochemistry, Geophysics, Geosystems 3*, 1 of 7-7 of 7.

Söderlund, U., Klausen, M. B., Ernst, R. E. & Bleeker, W., 2016: New advances in using large igneous provinces (LIPs) to reconstruct ancient supercontinents. *Gff*.

Srivastava, R. K., Söderlund, U., Ernst, R. E., Mondal, S. K. & Samal, A. K., 2019: Precambrian mafic dyke swarms in the Singhbhum craton (eastern India) and their links with dyke swarms of the eastern Dharwar craton (southern India). *Precambrian Research 329*, 5-17.

Sun, S.-S. & Mcdonough, W. F., 1989: Chemical and isotopic systematics of oceanic basalts: implications for mantle composition and processes. *J Geological Society, London, Special Publications 42*, 313-345.

Wabo, H., Humbert, F., De Kock, M., Belyanin, G., Söderlund, U., Maré, L. & Beukes, N. 2019: Constraining the chronology of the Mashishing dykes from the eastern Kaapvaal craton in South Africa. *In Dyke Swarms of the World: A Modern Perspective*, 215-261. Springer,

Walraven, F., 1997: *Geochronology of the Rooiberg Group, Transvaal Supergroup, South Africa*. Economic Geology Research Unit, University of the Witwatersrand.

Warke, M. R. & Schröder, S., 2018: Synsedimentary fault control on the deposition of the Duitschland Formation (South Africa): Implications for depositional settings, Paleoproterozoic stratigraphic correlations, and the GOE. *Precambrian Research 310*, 348-364.

Zeh, A., Ovtcharova, M., Wilson, A. H. & Schaltegger, U., 2015: The Bushveld Complex was emplaced and cooled in less than one million years–results of zirconology, and geotectonic

Tidigare skrifter i serien ”Examensarbeten i Geologi vid Lunds universitet”:

523. Christensson, Lisa, 2017: Geofysisk undersökning av grundvattenskydd för planerad reservvattentäkt i Mjölkalånga, Hässleholms kommun. (15 hp)
524. Stamsnijder, Joaen, 2017: New geochronological constraints on the Klipriviersberg Group: defining a new Neoarchean large igneous province on the Kaapvaal Craton, South Africa. (45 hp)
525. Becker Jensen, Amanda, 2017: Den eocena Furformationen i Danmark: exceptionella bevaringstillstånd har bidragit till att djurs mjukdelar fossiliserats.(15 hp)
526. Radomski, Jan, 2018: Carbonate sedimentology and carbon isotope stratigraphy of the Tallbacken-1 core, early Wenlock Slite Group, Gotland, Sweden. (45 hp)
527. Pettersson, Johan, 2018: Ultrastructure and biomolecular composition of sea turtle epidermal remains from the Campanian (Upper Cretaceous) North Sulphur River of Texas. (45 hp)
528. Jansson, Robin, 2018: Multidisciplinary perspective on a natural attenuation zone in a PCE contaminated aquifer. (45 hp)
529. Larsson, Alfred, 2018: Rb-Sr sphalerite data and implications for the source and timing of Pb-Zn deposits at the Caledonian margin in Sweden. (45 hp)
530. Balija, Fisnik, 2018: Stratigraphy and pyrite geochemistry of the Lower–Upper Ordovician in the Lerhamn and Fågelsång -3 drill cores, Scania, Sweden. (45 hp)
531. Höglund, Nikolas, 2018: Groundwater chemistry evaluation and a GIS-based approach for determining groundwater potential in Mörbylånga, Sweden. (45 hp)
532. Haag, Vendela, 2018: Studie av mikrostrukturer i karbonatslagkäglor från nedslagsstrukturen Charlevoix, Kanada. (15 hp)
533. Hebrard, Benoit, 2018: Antropocen – vad, när och hur? (15 hp)
534. Jancsak, Nathalie, 2018: Åtgärder mot kusterosion i Skåne, samt en fallstudie av erosionsskydden i Löderup, Ystad kommun. (15 hp)
535. Zachén, Gabriel, 2018: Mesosideriter – redogörelse av bildningsprocesser samt SEM-analys av Vaca Muertameteoriten. (15 hp)
536. Fägersten, Andreas, 2018: Lateral variability in the quantification of calcareous nannofossils in the Upper Triassic, Austria. (15 hp)
537. Hjertman, Anna, 2018: Förutsättningar för djupinfiltration av ytvatten från Ivösjön till Kristianstadbassängen. (15 hp)
538. Lagerstam, Clarence, 2018: Varför svalde svanödlor (Reptilia, Plesiosauria) stenar? (15 hp)
539. Pilser, Hannes, 2018: Mg/Ca i bottenlevande foraminiferer, särskilt med avseende på temperaturer nära 0°C. (15 hp)
540. Christiansen, Emma, 2018: Mikroplast på och i havsbotten - Utbredningen av mikroplaster i marina bottensediment och dess påverkan på marina miljöer. (15 hp)
541. Staahlnacke, Simon, 2018: En sammanställning av norra Skånes prekambriska berggrund. (15 hp)
542. Martell, Josefin, 2018: Shock metamorphic features in zircon grains from the Mien impact structure - clues to conditions during impact. (45 hp)
543. Chitindingu, Tawonga, 2018: Petrological characterization of the Cambrian sandstone reservoirs in the Baltic Basin, Sweden. (45 hp)
544. Chonewicz, Julia, 2018: Dimensionerande vattenförbrukning och alternativa vattenkvaliteter. (15 hp)
545. Adeen, Lina, 2018: Hur lämpliga är de geofysiska metoderna resistivitet och IP för kartläggning av PFOS? (15 hp)
546. Nilsson Brunlid, Anette, 2018: Impact of southern Baltic sea-level changes on landscape development in the Verkeån River valley at Haväng, southern Sweden, during the early and mid Holocene. (45 hp)
547. Perälä, Jesper, 2018: Dynamic Recrystallization in the Sveconorwegian Frontal Wedge, Småland, southern Sweden. (45 hp)
548. Artursson, Christopher, 2018: Stratigraphy, sedimentology and geophysical assessment of the early Silurian Halla and Klinteberg formations, Altajme core, Gotland, Sweden. (45 hp)
549. Kempengren, Henrik, 2018: Att välja den mest hållbara efterbehandlingsmetoden vid sanering: Applicering av beslutsstödsverktyget SAMLA. (45 hp)
550. Andreasson, Dagnija, 2018: Assessment of using liquidity index for the approximation of undrained shear strength of clay tills in Scania. (45 hp)
551. Ahrenstedt, Viktor, 2018: The Neoproterozoic Visingsö Group of southern Sweden: Lithology, sequence stratigraphy and provenance of the Middle Formation. (45 hp)
552. Berglund, Marie, 2018: Basaltkuppen - ett spel om mineralogi och petrologi. (15 hp)
553. Hernnäs, Tove, 2018: Garnet amphibolite in the internal Eastern Segment, Sveconorwegian Province: monitors of

metamorphic recrystallization at high temperature and pressure during Sveconorwegian orogeny. (45 hp)

554. Halling, Jenny, 2019: Characterization of black rust in reinforced concrete structures: analyses of field samples from southern Sweden. (45 hp)
555. Stevic, Marijana, 2019: Stratigraphy and dating of a lake sediment record from Lyngsjön, eastern Scania - human impact and aeolian sand deposition during the last millennium. (45 hp)
556. Rabanser, Monika, 2019: Processes of Lateral Moraine Formation at a Debris-covered Glacier, Suldenferner (Vedretta di Solda), Italy. (45 hp)
557. Nilsson, Hanna, 2019: Records of environmental change and sedimentation processes over the last century in a Baltic coastal inlet. (45 hp)
558. Ingered, Mimmi, 2019: Zircon U-Pb constraints on the timing of Sveconorwegian migmatite formation in the Western and Median Segments of the Idefjorden terrane, SW Sweden. (45 hp)
559. Hjorth, Ingeborg, 2019: Paleomagnetisk undersökning av vulkanen Rangitoto, Nya Zeeland, för att bestämma dess utbrottshistoria. (15 hp)
560. Westberg, Märta, 2019: Enigmatic worm-like fossils from the Silurian Waukesha Lagerstätte, Wisconsin, USA. (15 hp)
561. Björn, Julia, 2019: Undersökning av påverkan på hydraulisk konduktivitet i förorenat område efter in situ-saneringsförsök. (15 hp)
562. Faraj, Haider, 2019: Tolkning av georadarprofiler över grundvattenmagasinet Verveln - Gullringen i Kalmar län. (15 hp)
563. Bjermo, Tim, 2019: Eoliska avlagringar och vindriktningar under holocen i och kring Store Mosse, södra Sverige. (15 hp)
564. Langkjaer, Henrik, 2019: Analys av Östergötlands kommande grundvattenresurser ur ett klimtperspektiv - med fokus på förstärkt grundvattenbildning. (15 hp)
565. Johansson, Marcus, 2019: Hur öppet var landskapet i södra Sverige under Atlantisk tid? (15 hp)
566. Molin, Emmy, 2019: Litologi, sedimentologi och kolisotopstratigrafi över krita–paleogen-gränsintervallet i borrningen Limhamn-2018. (15 hp)
567. Schroeder, Mimmi, 2019: The history of European hemp cultivation. (15 hp)
568. Damber, Maja, 2019: Granens invandring i sydvästa Sverige, belyst genom pollenanalys från Skottenesjön. (15 hp)
569. Lundgren Sassner, Lykke, 2019: Strandmorfologi, stranderosion och stranddeposition, med en fallstudie på Tylösand sandstrand, Halland. (15 hp)
570. Greiff, Johannes, 2019: Mesozoiska konglomerat och Skånes tektoniska utveckling. (15 hp)
571. Persson, Eric, 2019: An Enigmatic Cerapodian Dentary from the Cretaceous of southern Sweden. (15 hp)
572. Aldenius, Erik, 2019: Subsurface characterization of the Lund Sandstone – 3D model of the sandstone reservoir and evaluation of the geoenergy storage potential, SW Skåne, South Sweden. (45 hp)
573. Juliusson, Oscar, 2019: Impacts of subglacial processes on underlying bedrock. (15 hp)
574. Sartell, Anna, 2019: Metamorphic paragenesis and P-T conditions in garnet amphibolite from the Median Segment of the Idefjorden Terrane, Lilla Edet. (15 hp)
575. Végvári, Fanni, 2019: Vulkanisk inverkan på klimatet och atmorsfärcirkulationen: En litterarurstudie som jämför vulkanism på låg respektive hög latitud. (15 hp)
576. Gustafsson, Jon, 2019: Petrology of platinum-group element mineralization in the Koillismaa intrusion, Finland. (45 hp)
577. Wahlquist, Per, 2019: Undersökning av mindre förkastningar för vattenuttag i sedimentärt berg kring Kingelstad och Tjutebro. (15 hp)
578. Gaitan Valencia, Camilo Esteban, 2019: Unravelling the timing and distribution of Paleoproterozoic dyke swarms in the eastern Kaapvaal Craton, South Africa. (45 hp)

LUNDS UNIVERSITET

Geologiska institutionen
Lunds universitet
Sölvegatan 12, 223 62 Lund